

METEORITICS & PLANETARY SCIENCE

**Heating experiments of the Tagish Lake meteorite:
investigation of the effects of short-term heating on
chondritic organics**

Journal:	<i>Meteoritics & Planetary Science</i>
Manuscript ID	MAPS-2971.R1
Manuscript Type:	Article
Date Submitted by the Author:	n/a
Complete List of Authors:	<p>Chan, Queenie Hoi Shan Nakato, Aiko; Kyoto University Kebukawa, Yoko; Carnegie Institution of Washington, Geophysical Laboratory Zolensky, Michael; NASA Johnson Space Center, Nakamura, Tomoki; Tohoku University, Department of Earth and Planetary Materials Science, Faculty of Science Maisano, Jessie; U T Austin, Colbert, Matthew ; U T Austin Martinez, James; Jacobs, Kilcoyne, David; LBNL, SSG Suga, Hiroki; Hiroshima University, Department of Earth and Planetary Systems Science Takahashi, Yoshio ; The University of Tokyo, Department of Earth and Planetary Science Takeichi, Yasuo; High-Energy Accelerator Research Organization ; Graduate University for Advanced Studies Mase, Kazuhiko; High-Energy Accelerator Research Organization ; Graduate University for Advanced Studies Wright, Ian; Open University, Physical Sciences</p>
Keywords:	Organic matter, Spectroscopy, alteration < Thermal, Space mission(s)
<p>Note: The following files were submitted by the author for peer review, but cannot be converted to PDF. You must view these files (e.g. movies) online.</p>	
<p>Movie S1.avi Movie S2.avi</p>	

SCHOLARONE™
Manuscripts

1
2
3
4 **1 Heating experiments of the Tagish Lake meteorite: investigation of the effects of**
5 **2 short-term heating on chondritic organics**
6

7
8 Queenie H. S. Chan^{1*†}, Aiko Nakato², Yoko Kebukawa³, Michael E. Zolensky¹,
9
10 Tomoki Nakamura⁴, Jessica A. Maisano⁵, Matthew W. Colbert⁵, James E. Martinez⁶,
11
12 A.L. David Kilcoyne⁷, Hiroki Suga⁸, Yoshio Takahashi⁹, Yasuo Takeichi^{10,11},
13
14 Kazuhiko Mase^{10,11} and Ian P. Wright¹
15

16
17
18
19
20
21
22
23
24
25
26
27
28
29
30
31
32
33
34
35
36
37
38
39
40
41
42
43
44
45
46
47
48
49
50
51
52
53
54
55
56
57

8 ¹ARES, NASA Johnson Space Center, Houston, Texas 77058, USA

9 ²Graduate School of Science, Kyoto University, Kitashirakawa Oiwake-cho, Sakyo-
10
11 ku, Kyoto 606-8502, Japan

11 ³Faculty of Engineering, Yokohama National University, 79-5 Tokiwadai,
12
13 Hodogayaku, Yokohama 240-8501, Japan

13 ⁴Graduate School of Science, Tohoku University, Sendai, Miyagi 980-8578, Japan

14 ⁵Department of Geological Sciences, Jackson School of Geosciences, The University
15
16 of Texas, Austin, TX 78712, USA

16 ⁶Jacobs Engineering, Houston, TX 77058, USA

17 ⁷Advanced Light Source, Lawrence Berkeley National Laboratory, 1 Cyclotron Road,
18
19 Berkeley, CA 94720, USA

19 ⁸Department of Earth and Planetary Systems Science, Hiroshima University,
20
21 Kagamiyama, Higashi-Hiroshima, Hiroshima 739-8526, Japan

21 ⁹Department of Earth and Planetary Science, The University of Tokyo, Hongo,
22
23 Bunkyo-ku, Tokyo 113-0033, Japan

23 ¹⁰Institute of Materials Structure Science, High-Energy Accelerator Research
24
25 Organization (KEK), 1-1 Oho, Tsukuba, Ibaraki 305-0801, Japan

25 ¹¹Department of Materials Structure Science, SOKENDAI (The Graduate University
26
27 for Advanced Studies)

28
29
30
31
32
33
34
35
36
37
38
39
40
41
42
43
44
45
46
47
48
49
50
51
52
53
54
55
56
57
58
59
60

28 *Corresponding author: Queenie H. S. Chan (E-mail: queenie.chan@open.ac.uk;
29
30 Telephone: +1 (585) 653-6144).

1
2
3 30 †Current address: Department of Physical Sciences, The Open University, Walton
4
5 31 Hall, Milton Keynes, MK7 6AA, UK
6
7 32
8
9
10
11
12
13
14
15
16
17
18
19
20
21
22
23
24
25
26
27
28
29
30
31
32
33
34
35
36
37
38
39
40
41
42
43
44
45
46
47
48
49
50
51
52
53
54
55
56
57
58
59
60

For Peer Review Only

33 **ABSTRACT**

34 We present in this study the effects of short-term heating on organics in the
35 Tagish Lake meteorite and how the difference in the heating conditions can modify
36 the organic matter (OM) in a way that complicates the interpretation of a parent
37 body's heating extent with common cosmothermometers. The kinetics of short-term
38 heating and its influence on the organic structure are not well understood, and any
39 study of OM is further complicated by the complex alteration processes of the
40 thermally metamorphosed carbonaceous chondrites – potential analogues of the target
41 asteroid Ryugu of the Hayabusa2 mission – which had experienced post-hydration,
42 short-duration local heating. In an attempt to understand the effects of short-term
43 heating on chondritic OM, we investigated the change in the OM contents of the
44 experimentally heated Tagish Lake meteorite samples using Raman spectroscopy,
45 scanning transmission X-ray microscopy utilizing X-ray absorption near edge
46 structure spectroscopy, and ultra-performance liquid chromatography fluorescence
47 detection and quadrupole time of flight hybrid mass spectrometry. Our experiment
48 suggests that graphitization of OM did not take place despite the samples being heated
49 to 900°C for 96 hours, as the OM maturity trend was influenced by the nature of the
50 OM precursor, such as the presence of abundant oxygenated moieties. Although both
51 the intensity of the $1s-\sigma^*$ exciton cannot be used to accurately interpret the peak
52 metamorphic temperature of the experimentally heated Tagish Lake sample, the
53 Raman graphite band widths of the heated products significantly differ from that of
54 chondritic OM modified by long-term internal heating.

55 1 INTRODUCTION

56 Carbonaceous chondrites exhibit a wide range of aqueous and thermal
57 alteration characteristics, while some are known to demonstrate mineralogical and
58 petrologic evidence of having been thermally metamorphosed after aqueous alteration.
59 Their occurrences challenge the initial view of which carbonaceous chondrites, that
60 have experienced pervasive aqueous alteration, were not extensively heated. This
61 group of dehydrated meteorites are commonly referred as thermally metamorphosed
62 carbonaceous chondrites (TMCCs), and their relatively flat visible near infrared
63 reflectance spectra resemble that of C-, G-, B- and F-type asteroids that typically have
64 low albedos (Gaffey et al. 1989; Hiroi et al. 1993; Hiroi et al. 1996). The surfaces of
65 these dark asteroids, which include the C- and B-type target asteroids – Ryugu and
66 Bennu of the ongoing sample return missions, Hayabusa2 and OSIRIS-REx,
67 respectively – are potentially composed of both hydrous and dehydrated minerals, and
68 thus TMCCs are among the best samples that can be studied in the laboratory to
69 reveal the true nature of these carbonaceous asteroids.

70 Although many TMCCs were previously categorized as Ivuna-type (CI) and
71 Mighei-type (CM) chondrites, they are not strictly CI/CM because they exhibit
72 isotopic and petrographic characteristics that significantly deviate from typical CI/CM,
73 and hence were given the term “CI-/CM-like chondrites”. TMCCs consist mainly of
74 dehydrated phyllosilicates, have higher bulk O isotopic compositions (CI-/CM-like
75 chondrites: $\delta^{17}\text{O} = +9$ to 12% , $\delta^{18}\text{O} = +17$ to 22% ; CM chondrites: $\delta^{17}\text{O} = -1$ to $+3\%$,
76 $\delta^{18}\text{O} = +5$ to 11%), and lower H₂O and C contents relative to CI/CM chondrites
77 (Clayton and Mayeda 1999; Ikeda 1992; Tonui et al. 2014). Examples of TMCCs
78 include the C2-ung/CM2TIV Belgica (B)-7904, Yamato (Y-), Y-82162, Y-86720, Y-
79 980115 and Wisconsin Range (WIS) 91600 (e.g., Akai 1988; Burton et al. 2014; Chan
80 et al. 2016a; Ikeda 1991, 1992; King et al. 2015b; Nakamura 2005; Nakato et al.
81 2008; Tomeoka et al. 1989a, b; Tonui et al. 2014). Thermal alteration is virtually
82 complete in B-7904 and Y-86720, thus they are considered typical end-members of
83 TMCCs exhibiting complete dehydration of matrix phyllosilicates (Nakamura 2005;
84 Tonui et al. 2014). The estimated heating durations of TMCCs are surprisingly short
85 when compared to parent body heating with heat sources derived from *in situ* decay of
86 radionuclides that could last millions of years. The heating conditions of TMCCs

1
2
3 87 were estimated to be 10 to 10³ days at 700°C to 1 to 100 hours at 890°C, which
4 suggest that they have experienced short-term heating possibly induced by impact
5 and/or solar radiation (Chan et al. 2017b; Nakato et al. 2008; Yabuta et al. 2010).
6
7

8
9 90 While the petrology and chemistry of TMCCs have only recently been
10 extensively characterized, we have just begun to study in detail how short-term
11 heating influences their organic contents. We investigated the change in the organic
12 content of the carbonate-poor lithology of experimentally heated Tagish Lake C2
13 meteorite, as the chemical and bulk oxygen (O) isotopic compositions ($\delta^{17}\text{O} = +8$ to
14 9%, $\delta^{18}\text{O} = +18$ to 19‰) of this lithology bear similarities to that of the TMCCs
15 (Clayton and Mayeda 2001; Engrand et al. 2001; Zolensky et al. 2002). The Tagish
16 Lake meteorite has a bulk carbon (C) content of approximately 4 wt%, of which about
17 <2 wt% comes from IOM and <1 wt% from carbonate C (Alexander et al. 2014;
18 Pearson et al. 2006). Carbonates are relatively uncommon in the carbonate-poor
19 lithology which occur as sparse fine polycrystalline grains of <5 μm (Zolensky et al.
20 2002), so the contribution of carbonate C to the bulk C content is expected to be lower
21 in this lithology. The carbonate-poor lithology also contains abundant organic
22 nanoglobules with aliphatic and oxygenated function groups that have elevated δD
23 and $\delta^{15}\text{N}$ values, which suggests a highly primitive, possibly presolar origin for the
24 organics, and their formation in the cold molecular clouds and the outer protosolar
25 disk at extremely low temperatures (<-250°C) (Nakamura-Messenger et al. 2006;
26 Nakamura et al. 2002). The bulk O isotopic composition and the presence of organic
27 nanoglobules indicate that aqueous alteration occurred at low temperatures (<100°C)
28 (Zolensky et al. 2002). The isotopic compositions ($\delta\text{D} = +815$ to 1844‰, $\delta^{13}\text{C} = -$
29 14.7 to -13.3 ‰, $\delta^{15}\text{N} = +53$ to 57) of the IOM extracted from the Tagish Lake
30 meteorite are intermediate between that of the IOM in typical CI, CM and Renazzo-
31 type (CR) chondrites (Alexander et al. 2014; Herd et al. 2011). The more aqueously-
32 altered lithology are drawn closer to the least metamorphosed ordinary chondrites
33 (OC), Vigarano-type (CV), and Ornans-type (CO) chondrites, which suggests that the
34 isotopic variation was to a certain extent influenced by aqueous alteration.
35 Nevertheless, only limited changes were observed for the C content, isotopic, and
36 structural properties of the IOM in the Tagish Lake meteorite samples that exhibit
37 different extents of aqueous alteration, which offers another line of evidence towards
38 a low temperature alteration history (Alexander et al. 2014; Yabuta et al. 2007).
39
40
41
42
43
44
45
46
47
48
49
50
51
52
53
54
55
56
57
58
59
60

1
2
3 120 The low temperature aqueous alteration history of the Tagish Lake meteorite,
4
5 121 its moderate IOM abundance relatively unaltered by aqueous processing, and its quick
6
7 122 retrieval (frozen) upon an observed fall event without direct hand contact (Brown et al.
8
9 123 2000), justify this meteorite as the perfect and organically pristine candidate for the
10
11 124 study of the change in the OM content by experimental heating. With the use of
12
13 125 Raman spectroscopy, scanning transmission X-ray microscopy (STXM) utilizing X-
14
15 126 ray absorption near edge structure (XANES) spectroscopy, and ultra-performance
16
17 127 liquid chromatography fluorescence detection and quadrupole time of flight hybrid
18
19 128 mass spectrometry (UPLC-FD/QToF-MS), we analyzed the compositions of the
20
21 129 organic solids and the amino acid contents of the experimentally heated (short-term
22
23 130 heating) Tagish Lake samples in detail.
24
25
26
27
28
29
30
31
32
33
34
35
36
37
38
39
40
41
42
43
44
45
46
47
48
49
50
51
52
53
54
55
56
57
58
59
60

132 2 SAMPLES AND METHODS

133 The Tagish Lake meteorite has two main lithologies – carbonate-poor (the
134 dominant lithology) and carbonate-rich (less abundant lithology) (Zolensky et al.
135 2002) (Figure 1). Different Tagish Lake meteorite fragments also exhibit a wide
136 variation in the organic content that correlates to the extent of parent body aqueous
137 alteration (Tagish Lake specimens showing an increasing degree of aqueous
138 alteration: 5b [the least aqueously altered] < 11h < 11i < 11v [the most aqueously
139 altered]), where the amino acid abundances are higher in the fragments which show a
140 lower degree of aqueous alteration, while the IOM C contents only decrease slightly
141 with a considerable increase in the aromatic content in the more aqueously-altered
142 lithology (e.g., Alexander et al. 2014; Glavin et al. 2012; Herd et al. 2011).

143 To ensure that our heating experiments and the interpretation of the resulting
144 organic content were not significantly influenced by sample heterogeneity, we
145 selected only the carbonate-poor lithology of the Tagish Lake meteorite (#11). The
146 carbonate-poor lithology was located by mineral identification via X-ray computed
147 tomography (XRCT) at the High-Resolution X-ray Computed Tomography Facility at
148 The University of Texas at Austin. Tomographic imaging was critical in identifying
149 internal lithologic and mineralogical differences, which we used to decide where to
150 make the initial slice into the sample and prepare thin sections. The initial samples
151 were then characterized by scanning electron microscopy (SEM) and energy-
152 dispersive spectrometry (EDS) to verify the carbonate-poor lithology based on
153 elemental mapping and comparison to the XRCT images (Figure 1).

154 We then subsampled the carbonate-poor lithology into four equal portions,
155 each weighing approximately 200 mg. Half of the samples was used in this study,
156 while the other half was analyzed to determine the variation in chemical, petrography,
157 mineralogy, and bulk O isotope compositions upon heating, using synchrotron X-ray
158 diffraction (XRD) analysis at the High Energy Accelerator Research Organization
159 (KEK) using beam line BL-3A, and SEM/EDS, electron probe micro-analyzer
160 equipped with a wavelength dispersive spectrometer (EPMA/WDS), transmission
161 electron microscopy (TEM) and laser fluorination mass spectrometer at JAXA/ISAS.
162 The results of the second portion of the sample are discussed in Nakato et al. (2016).

163 2.1 XRCT

1
2
3 164 The Tagish Lake meteorite sample was scanned at the University of Texas
4
5 165 High-Resolution X-ray Computed Tomography Facility using the Xradia microXCT
6
7 166 Scanner (Zeiss). The detector permits cone-beam acquisition, and under the ultra
8
9 167 high-resolution mode, 882 slices were collected covering the entire scan volume in a
10
11 168 single rotation. Images were obtained by relatively low-energy X-rays (80kV), 10W,
12
13 169 2.5 s acquisition time, with a spatial resolution (voxel size) of 46 μm .

14 15 170 **2.2 SEM/EDS**

16
17 171 Secondary electron (SE) imaging and mineral elemental compositions were
18
19 172 obtained using the Zeiss SUPRA 55VP field-emission (FE) SEM at the Structural
20
21 173 Engineering Division, NASA Johnson Space Center (JSC) (Figure S1). Fragments of
22
23 174 the Tagish Lake meteorite were mounted in indium and prepared in the same manner
24
25 175 as described in Chan et al. (2016b). The SEM parameters were: Accelerating voltage
26
27 176 = 20 kV; Aperture = 120 mm (largest); High current mode = on; Beam size =
28
29 177 approximately 3 to 5 nm; Incident beam current = 9.2 to 9.3 nA; Working distance \approx 6
30
31 178 mm.

32 33 179 **2.3 Heating experiments**

34
35 180 Subsamples (\sim 100 mg) of the carbonate-poor Tagish Lake lithology were
36
37 181 subjected to heating experiments at 600° and 900°C for 1 and 96 hours: (1) 600°C/1h,
38
39 182 (2) 600°C/96h, (3) 900°C/1h, and (4) 900°C/96h. During the experiments, the heating
40
41 183 chamber was kept under a controlled environment. To reproduce the secondary iron-
42
43 184 bearing minerals in B-7904 heated chondrite that contains both Fe and Fe²⁺, a Fe
44
45 185 metal rod was put in the chamber with the O fugacity kept at the condition closer to
46
47 186 that of the iron-wüstite (IW) buffer. The estimated pressure was below 5×10^{-5} Pa.
48
49 187 The detailed experimental configuration is shown in Nakato et al. (2008).

50 51 188 **2.4 Raman spectroscopy**

52
53 189 The unheated and heated Tagish Lake samples were analyzed using a Jobin-
54
55 190 Yvon Horiba LabRam HR (800 mm) Raman microprobe at NASA JSC. The
56
57 191 excitation source was a 514 nm (green) laser. The slit width and the confocal pinhole
58
59 192 aperture were set at 100 μm and 200 μm , respectively, and an 1800 grooves/mm
60
193 grating was used to disperse the Raman signal. The laser beam was focused through a
194
194 194 microscope equipped with an 80 \times objective (numerical aperture = 0.75), and the

1
2
3 195 Raman backscattered light was collected from the same objective. At this
4
5 196 magnification and for the laser used, the minimum achievable spot size was
6
7 197 approximately 1 μm , and the laser power at the sample surface was $\leq 450 \mu\text{W}$. At least
8
9 198 12 spectra were collected on each raw matrix grain (flattened between two glass
10
11 199 slides) in the spectral range of 100–4000 cm^{-1} . This spectral range includes the first-
12
13 200 and second-order Raman bands of carbon. The exposure time for each spectrum was
14
15 201 15s and three accumulations were obtained for each analytical spot to identify and
16
17 202 discard spurious signals, such as those from cosmic rays, leading to a total acquisition
18
19 203 time of up to 450 s with the use of an Extended Range option to collect data in various
20
21 204 spectral windows.

22
23 205 The peak position (ω) and full width half-maximum (FWHM, Γ) of each
24
25 206 Raman band were determined by simultaneous peak fitting to the two-peak
26
27 207 Lorentzian and Breit–Wigner-Fano (BWF) model (Ferrari and Robertson 2000) with a
28
29 208 linear baseline correction (Figure S2 and Figure S3). Wavelength calibration against a
30
31 209 silicon wafer sample was checked daily prior to sample analyses. Details of the
32
33 210 Raman technique are given in Chan et al. (2017b) and Kebukawa et al. (2017).

34 211 **2.5 STXM-XANES**

35 212 Focused ion beam (FIB) thin sections of the heated and unheated Tagish Lake
36
37 213 samples were prepared using a FIB (Hitachi, FB2200) at ISAS/JAXA for three
38
39 214 STXM-XANES analyses (2016 Feb, 2016 May and 2016 Dec). We subsampled FIB
40
41 215 sections for each STXM-XANES analysis in order to investigate the sample
42
43 216 heterogeneity. C-XANES measurements were performed using the compact-STXM
44
45 217 installed at BL-13A beamline of the Photon Factory (PF), High Energy Accelerator
46
47 218 Research Organization (KEK), and the STXM installed at beamline 5.3.2.2 of the
48
49 219 Advanced Light Source, Lawrence Berkeley National Laboratory. The details of these
50
51 220 instruments are described in Kilcoyne et al. (2003) and Takeichi et al. (2016). The C-
52
53 221 XANES spectra were acquired using a “Stacks” method, with the energy step sizes of
54
55 222 0.1 eV in the region of 283–295.5 eV, 0.5 eV in the regions of 280–283 eV and
56
57 223 295.5–301.0 eV, and 1 eV in the region of 301–310 eV. The acquisition time for each
58
59 224 energy step varied from 1 to 5 ms. The C-XANES spectra were corrected with
60
225 background and analyzed by the subtraction of a linear regression using aXis2000
226 software, and then normalized to the intensity at 292 eV.

227 2.6 UPLC-FD/QToF-MS

228 The amino acid extraction was conducted at NASA JSC in the same manner as
229 described in Chan et al. (2018). Porcelain mortars and pestles were scrubbed and
230 washed with dilute soap solution, rinsed with Millipore Integral 10 UV (18.2 M Ω cm,
231 <3 parts-per-billion [ppb] total organic carbon) ultrapure water, hereafter referred to
232 as “water”, immersed in 20% citric acid and sonicated at room temperature for 60 min.
233 All tools, glassware, and ceramics were rinsed with water, wrapped in aluminum foil,
234 and sterilized by heating in air at 500 °C for 24 h. Volumetric flasks were only rinsed
235 with copious water. Amino acid standards and other laboratory chemicals such as
236 ammonium hydroxide (NH₄OH) (28–30 wt %), sodium hydroxide (NaOH),
237 hydrochloric acid (HCl) (37 %), methanol, hydrazine monohydrochloride, *o*-
238 phthaldialdehyde (OPA), *N*-acetyl-L-cysteine (NAC) were obtained from Fischer
239 Scientific, Sigma-Aldrich, or Acros Organics. Poly-Prep® prepacked ion exchange
240 columns (AG 50W-X8 resin, 200–400 mesh, hydrogen form) were obtained from
241 Bio-Rad. Solutions of sodium borate were prepared from solid sodium tetraborate
242 decahydrate (Sigma Ultra 99.5–100% purity) that was heated in air at 500 °C for 24 h
243 prior to dissolution in water. Amino acid standard solutions were made by dissolving
244 individual amino acid solutes in water, and were combined into a standard mixture
245 analyzed by UPLC-FD/QToF-MS on a daily basis.

246 The unheated and heated Tagish Lake meteorite samples were powdered and
247 transferred to individual glass ampoules. Sterilized (500°C, 24h) laboratory quartz
248 samples were subjected to the same heating experiment and amino acid extraction
249 procedures and analyzed as procedural blanks.

250 One mL of water was added to each glass ampoule containing separate
251 samples, and the ampoules were flame-sealed and heated to 100 °C for 24 h in an
252 oven. After the hot water extraction, the samples were cooled to room temperature
253 and centrifuged for 5 min to separate water supernatant from solid particulate. Exactly
254 half of the water supernatant (500 μ L) was transferred to a small test tube (10 \times 75
255 mm), dried under vacuum (Savant™ SPD131DDA SpeedVac™ Concentrator),
256 flame-sealed in a larger test tube (20 \times 150 mm) containing 6 N HCl, and then
257 subjected to acid vapor hydrolysis for 3 h at 150 °C in order to liberate amino acids in
258 bound or precursor forms. After the vapor-hydrolysis procedure, the test tubes were

1
2
3 259 rinsed with water, and the bottom of the test tubes were opened to retrieve the inner
4
5 260 small test tubes, and this portion of the sample is hereafter referred to as the
6
7 261 “hydrolyzed extract”, representing the total amino acid contents of the samples. The
8
9 262 remaining hot-water extract was rinsed with 2×1 mL water and the supernatant was
10
11 263 transferred to individual test tubes, this portion of the sample is hereafter referred to
12
13 264 as the “non-hydrolyzed extract” (not described further in this study), containing only
14
15 265 the free amino acids. Both hydrolyzed and non-hydrolyzed samples were then brought
16
17 266 up in 3×1 mL of water and desalted on a cation exchange resin. Amino acids were
18
19 267 eluted with 2×3.5 mL of 2 M NH_4OH . The eluates were collected in small test tubes
20
21 268 and evaporated to dryness. The samples were transferred to small sample vials, re-
22
23 269 dissolved in 100 μL of water, and stored at -20°C . Immediately before UPLC-
24
25 270 FD/QToF-MS analysis, the samples were derivatized with OPA/NAC fluorescent
26
27 271 derivatization (Glavin et al. 2006). 25 μL of the thawed sample was dried under
28
29 272 vacuum, re-suspended in 20 μL 0.1 M sodium borate buffer (pH 9), and derivatized
30
31 273 with 5 μL OPA/NAC in 1 mL autosampler glass vials. The derivatization reaction was
32
33 274 then quenched after 15 min. at room temperature with 75 μL of 0.1 M hydrazine
34
35 275 hydrate.

36
37 276 The amino acid abundances and distributions were measured by UPLC-
38
39 277 FD/QToF-MS at NASA JSC, using a Waters ACQUITY ultrahigh performance LC
40
41 278 and a Waters ACQUITY fluorescence detector connected in series to a Waters LCT
42
43 279 Premier ToF-MS. 25 μL of the derivatized samples were separated using a Waters
44
45 280 BEH C18 column (2.1×50 mm, 1.7 μm particle size) followed by a second Waters
46
47 281 BEH phenyl column (2.1×150 mm, 1.7 μm particle size). Chromatographic
48
49 282 conditions were: column temperature, 30°C ; flow rate, 150 $\mu\text{L min}^{-1}$; solvent A (50
50
51 283 mM ammonium formate, 8% methanol, pH 8.0); solvent B (methanol); gradient, time
52
53 284 in minutes (%B): 0 (0), 35 (55), 45 (100). The electrospray and mass spectrometer
54
55 285 conditions have been described by Glavin et al. (2006). Amino acids in the samples
56
57 286 were identified by correlating sample compounds with known standards using the
58
59 287 representative masses and fluorescence responses of the OPA/NAC amino acid
60
288 derivatives at the expected chromatographic retention times.

289

290 3 RESULTS

291 The Tagish Lake meteorite fragments heated under the four experiments show
292 distinctive textural, mineralogical, structural, and chemical changes (Figure 2). The
293 mineralogy and texture of the Tagish Lake samples heated at 900°C show the closest
294 resemblance to that of the strongly heated TMCCs due to the dehydration of hydrous
295 minerals such as phyllosilicates and formation of magnetite, and recrystallization back
296 into anhydrous fine-grained (<100 nm) secondary olivine, pyroxene, Fe-Ni metal and
297 troilite (Nakato et al. 2016). Therefore, while phyllosilicates (e.g. saponite and
298 serpentine), magnetite and Fe-Ni sulfides are common mineral phases observed in the
299 matrix of the unheated carbonate-poor lithology of the Tagish Lake meteorite
300 (Zolensky et al. 2002), the Tagish Lake samples heated to 900°C show mineral
301 assemblages of predominantly anhydrous silicates, metal and troilite, implying a
302 reducing heating environment. Upon heating at 900°C, oxidation of organics by
303 silicate O has reduced the total C contents of the Tagish Lake samples down to
304 approximately 20% of that of the unheated counterpart, and thus the majority of the
305 IOM was decomposed after heating (T. Nakamura, personal communication, 2018).
306 This also accounts for the increase in the abundance of metallic Fe produced by the
307 reduction of silicate FeO. The changes in mineralogical and isotopic compositions are
308 discussed in more detail in a separate paper. In this paper, we focus on the changes
309 observed in the organic contents of the meteorite fragments.

310 3.1 Raman C parameters of the Tagish Lake OM

311 3.1.1 *OM in the unheated Tagish Lake meteorite*

312 Carbonaceous materials feature Raman bands in the first- and second-order
313 regions. The most typical peaks are the first-order defect (D) band at ~1350–1380 cm⁻¹
314 and the graphite (G) band at ~1580–1590 cm⁻¹ (Tuinstra and Koenig 1970a, b). The
315 peak parameters of the D and G bands, such as the peak center locations (usually
316 referred to as peak position, ω), peak widths in terms of full width half-maximum
317 (FWHM, Γ), and the peak intensity ratios between the D and G bands (I_D/I_G), were
318 documented to systematically correlate with various properties of OM in meteorites.
319 The combination of these peak parameters describes the overall size distribution of
320 the crystalline domains and the metamorphic history of the carbonaceous host (Aoya
321 et al. 2010; Beyssac et al. 2002; Bonal et al. 2006; Bonal et al. 2007; Busemann et al.

1
2
3 322 2007; Chan et al. 2017b; Homma et al. 2015; Kouketsu et al. 2014; Quirico et al.
4
5 323 2003).

6
7 324 Due to the sample heterogeneity of the Tagish Lake meteorite (Zolensky et al.
8
9 325 2002), and the adoption of different analytical methods and peak fitting algorithm, the
10
11 326 Raman parameters of the OM in the Tagish Lake meteorite reported by different
12
13 327 studies (Busemann et al. 2007; Matrajt et al. 2004; Nakamura et al. 2002; Quirico et al.
14
15 328 2014) are not necessarily the same (Table S1). Nevertheless, all studies are in
16
17 329 agreement that the IOM in the Tagish Lake meteorite contains abundant, highly-
18
19 330 disordered organic material. We have also analyzed separately three of the unheated
20
21 331 subsamples from the carbonate-poor lithology of the Tagish Lake meteorite, and the
22
23 332 Raman peak parameters of the OM are consistent with this study (Figure 3).

23 333 *3.1.2 Heating experiments*

24
25 334 A reduction in the fluorescence background intensity was observed after the
26
27 335 Tagish Lake meteorite samples were subjected to the short-term heating experiments
28
29 336 (Figure 4a). The unheated Tagish Lake meteorite fragment has the highest Raman
30
31 337 intensity across the 100–4000 cm^{-1} spectral range, which is accompanied by an
32
33 338 intense fluorescence signal leading to a steep background slope in the first-order D
34
35 339 and G bands spectral region between 1300–1600 cm^{-1} . Accordingly, the I_D/I_G ratio
36
37 340 increases as the Tagish Lake meteorite sample was exposed to higher heating
38
39 341 temperatures (Figure 3b; Figure 4b). However, while the Raman band parameters
40
41 342 show a clear correlation to the heating temperature, heating duration affects these
42
43 343 parameters to a lesser extent. For instance, while samples heated to 900°C for 96h
44
45 344 (shown as the diagonal-line-patterned symbols in Figure 3) has a lower fluorescence
46
47 345 intensity, lower Γ_D and ω_D values than the 1h counterparts, this trend is opposite for
48
49 346 the samples heated to 600°C. The difference in the 1h and 96h heating durations
50
51 347 might not be significant enough to cause any observable variation in the Raman
52
53 348 signatures.

52 349 **3.2 C-XANES analysis of the Tagish Lake OM**

53 350 *3.2.1 OM in the unheated Tagish Lake meteorite*

54
55
56
57 351 C-XANES spectroscopy is useful for detecting organic functional groups
58
59 352 albeit incapable of characterizing the structure of the entire organic molecule. The
60

1
2
3 353 OM in the Tagish Lake meteorite bears similarities to the IOM in the highly primitive
4
5 354 CI, CR and CM carbonaceous chondrites (Alexander et al. 2014; Cody et al. 2008a;
6
7 355 Le Guillou et al. 2014), in terms of the types and relative abundance of the chemical
8
9 356 moieties. The C-XANES spectra of the unheated Tagish Lake meteorite sample
10
11 357 (Figure 5a) reveal an absorption feature at ~285.0 eV that is assigned to the $1s-\pi^*$
12
13 358 transition of alkenyl and aromatic (C=C) carbon (Cody et al. 2008a). The weak peak
14
15 359 at around 286.5 eV indicates a minor contribution of ketones (C=O), and at ~287.5 eV
16
17 360 indicates aliphatic carbon (CH_n). However, the 287.5 eV feature is not distinctive in
18
19 361 the Tagish Lake meteorite, probably due to (1) the small H/C and aliphatic/aromatic
20
21 362 ratios of the OM in the more aqueously-altered lithology of the Tagish Lake meteorite
22
23 363 compared to those of primitive CC (e.g., Alexander et al. 2014; Herd et al. 2011),
24
25 364 and/or (2) C-XANES is less sensitive to the aliphatic carbon in complex
26
27 365 macromolecular OM. The highly aromatic rich nature of the OM suggests that this
28
29 366 Tagish Lake sample is more comparable to the aqueously altered specimens such as
30
31 367 11v and 11i rather than 5b analyzed in previous studies (e.g., Herd et al. 2011). The
32
33 368 peak centered at ~288.5 eV corresponds to a $1s-\pi^*$ transition associated with carbonyl
34
35 369 carbon in carboxyl moieties and esters (O-C=O) (Lessard et al. 2007). In some
36
37 370 locations, a small peak at 290.5 eV can be observed, which is assigned to the $1s-\pi^*$ of
38
39 371 carbonate. Differences in the presence and intensities of the above-mentioned peaks
40
41 372 measured on different days on FIB sections extracted from adjacent areas of the same
42
43 373 sample chip indicate significant sample heterogeneity (Figure 5a).

44 374 3.2.2 *Heating experiments*

45 375 Due to the significant sample heterogeneity, it was difficult to directly
46
47 376 correlate any systematic variation in the organic structure to the extent of heating
48
49 377 (Figure 5). The aromatic feature (C=C) at ~285.0 eV was expected to be more
50
51 378 prominent in the heated samples as thermal annealing typically converts sp^3 C into
52
53 379 aromatic sp^2 C and leads to an increase in the size of the aromatic moieties (Derenne
54
55 380 and Robert 2010; Dischler et al. 1983). However, as shown in Figure 5b, the 285.0 eV
56
57 381 peak intensity of the 900°C samples (magenta and red lines) is not always higher than
58
59 382 the unheated (black lines) or the 600°C samples (blue and green lines). We have also
60
383 conducted C-XANES spectral fitting following the procedure described in (Bernard et
384
385 al. 2010) (Figure 6), derived from Gaussian fits to the major X-ray absorption features,
in order to provide better quantification estimates for the absorption band intensities.

1
2
3 386 An example of a decomposed spectrum is provided in Figure S4. However, we did not
4
5 387 observe any distinct trend among the peak area ratios (carboxyl to aliphatic, ketone to
6
7 388 aliphatic, and aromatic to aliphatic) across samples that were heated to different
8
9 389 extents, as any apparent trend observed were compensated by the error bars which
10
11 390 represent sample heterogeneity (Figure 6). In addition, no systematic change was
12
13 391 observed for the aliphatic (CH_n at ~ 287.5 eV) and graphene (at ~ 291.6 eV) structures
14
15 392 upon heating. A $1s\text{-}\sigma^*$ exciton peak is expected if highly conjugated sp^2 bonded C
16
17 393 domains were present, as in the long-term thermally metamorphosed type 3 chondrites
18
19 394 (Cody et al. 2008b), but the peak is absent in the C-XANES spectra of all the
20
21 395 experimentally heated Tagish Lake samples. Nevertheless, the apparent lack of trends
22
23 396 in the peak area ratio may be hidden by molecular transformation into polycyclic
24
25 397 aromatic hydrocarbons (PAHs) that shows several resonances at the range of 285–291
26
27 398 eV, in addition to main π^* transition at ~ 285 eV. For example, the 285–291 eV
28
29 399 regions of the C-XANES spectra of benzene (which has 3 π^* states) and anthracene
30
31 400 (which has 7 π^* states) are distinct from each other, as benzene has several minor
32
33 401 peaks between 287–291 eV in addition to a prominent broad peak at ~ 285 eV,
34
35 402 whereas anthracene is comparatively featureless between 287–291 eV while the main
36
37 403 feature at ~ 285 eV is shown as two smaller peaks at around 284 and 286 eV
38
39 404 respectively (Gordon et al. 2003). Therefore, while the intensity at ~ 287.5 eV is
40
41 405 reduced in response to the loss of aliphatic carbon in response to heating, heating also
42
43 406 simultaneously increases the size of polycyclic aromatic domains (increasing the
44
45 407 number of π^* states) that show different resonances across the 285–291 eV region of
46
47 408 the C-XANES spectrum, which could then lead to a non-systematic variation in the
48
49 409 peak area ratio.

410 3.3 Heating experiments – changes in the amino acid content

411 The procedural-blank-subtracted amino acid contents of the 6 M HCl-vapor
412 hydrolyzed, hot-water extracts from the unheated and experimentally heated Tagish
413 Lake meteorite samples show peaks that were identified by comparison with amino
414 acid standards, fluorescence, retention time, and mass (Figure 7 and Table 1). The
415 total amino acid abundance (free + bound) of the identified amino acids in the
416 unheated Tagish Lake sample was about 89 parts-per-billion (ppb), which is
417 consistent with the low amino acid abundance observed for the aqueously-altered

1
2
3 418 lithology of the Tagish Lake sample (sample 11i, 40–100 ppb) and other TMCCs (e.g.
4 419 Y-980115 ~300 ppb) in the literature (Burton et al. 2014; Chan et al. 2016a; Glavin et
5 420 al. 2012; Herd et al. 2011; Kminek et al. 2002; Pizzarello et al. 2001). The relative
6 421 amino acid abundance (normalized to glycine) of the unheated Tagish Lake sample is
7 422 also comparable to the aqueously-altered lithology of Tagish Lake (Figure 7).

8
9
10
11
12 423 It is often assumed that the abundance in the aliphatic moieties, including the
13 424 amino acid content, would be significantly reduced by decarboxylation or conversion
14 425 into aromatic C upon pyrolysis. Amino acids can be decomposed at temperatures as
15 426 low as 100°C (Pietrucci et al. 2018), while proteic-amino acids are typically more
16 427 thermodynamically unstable than non-proteic amino acids (e.g. β -alanine, γ -
17 428 aminobutyric acid [γ -ABA]) (Kitadai 2016). Therefore, heating up to 600–900°C is
18 429 expected to destroy amino acids through processes such as decarboxylation,
19 430 deamination and chain homolysis which can result in the formation of a variety of
20 431 simple volatile organic compounds such as amines, carboxylic acids and
21 432 hydrocarbons (e.g., Bada et al. 1995; Pietrucci et al. 2018; Ratcliff et al. 1974). While
22 433 the relative amino acid abundances are similar between the unheated and heated
23 434 Tagish Lake meteorite samples (Figure 7), the total (identified) amino acid
24 435 abundances of the heating experiment product increased by nearly tenfold from ~89
25 436 ppb in the unheated sample to ~760 ppb in the sample heated to 900°C for 96h. The
26 437 total abundances of the non-protein forming D-amino acids also increased by a factor
27 438 of 4–5 in the 900°C experiments. These results are completely unexpected as any
28 439 amino acid present in the samples are susceptible to thermal decomposition at high
29 440 temperatures. One possibility of the increase in the amino acid abundance subsequent
30 441 to heating, is that amino acids are formed from simple precursor molecules such as
31 442 CO, N₂ and H₂ which serve as feedstock for mineral-catalyzed Fischer Tropsch-type
32 443 (FTT) reactions (e.g., Anders et al. 1973; Pizzarello 2012; Yoshino et al. 1971). The
33 444 FTT reactions lead to the formation of primarily straight-chain amino acids (e.g.
34 445 glycine, β -alanine, γ -ABA, ϵ -amino-*n*-caproic acid [EACA]) of which the amino
35 446 group is on the carbon farthest from the carboxylic acid. However, when heated to
36 447 900°C, the minerals commonly associated with FTT reactions such as
37 448 montmorillonite clay and magnetite are at expense to form anhydrous silicates, metal
38 449 and troilite in the Tagish Lake samples (Figure 2). Although metals can also act as
39 450 FTT reactions catalysts (Dry 2002), hydrogenation of CO to hydrocarbons is a very

1
2
3 451 slow process in the absence of a suitable catalyst (Hayatsu and Anders 1981; Lancet
4 452 and Anders 1970). The mineral phases of which the formation thresholds are above
5 453 ~350–400K, such as olivine, Fe and FeS, are not effective catalysts for the FTT
6 454 reactions, whereas the phases formed at lower temperatures (e.g. montmorillonite clay
7 455 and magnetite) are. This elucidates a higher abundance of organic compounds in
8 456 meteorites containing these mineral phases. Therefore, the formation of amino acids
9 457 via the FTT reactions in the absence of these effective catalysts should be hindered
10 458 rather than enhanced. When focusing on the yield of the four-carbon amino acids
11 459 ABA, the abundances of the straight-chain γ -ABA are not always higher than that of
12 460 the branched isomers in the heated samples (Figure 7), which again testify against the
13 461 production of amino acids via the FTT reactions. The amino acid contents were
14 462 hampered by the enrichment in the L-enantiomers (e.g. the L-enantiomeric excesses
15 463 (L_{ee}) of aspartic acid in the unheated Tagish Lake sample = -1.3% and 900°C 96h
16 464 experiment product = 36.9%), and thus the other cause for the apparent increase in the
17 465 amino acid abundance is that the amino acids were potentially terrestrial contaminants,
18 466 possibly introduced via additional sample handling during the heating experiments.
19 467 Even though the aqueously-altered Tagish Lake sample is commonly known to
20 468 exhibit a large L_{ee} of ~45 to 99% for the proteic amino acids threonine, serine,
21 469 aspartic and glutamic acids (Glavin et al. 2012), it is difficult to completely eliminate
22 470 the possibility of a contribution from terrestrial contamination for this work, in
23 471 particular when compound-specific isotopic analysis was implausible due to the low
24 472 amino acid abundance in this lithology. In addition, Glavin et al. (2012) observed a
25 473 racemic ratio for the indigenous alanine in the Tagish Lake meteorite, and yet the
26 474 alanine in the experiments exhibits L_{ee} . Therefore, the carbonate-poor lithology of the
27 475 Tagish Lake meteorite in this study corresponds to the aqueously-altered counterparts
28 476 with very low amino acid abundance, and a confident interpretation of the change in
29 477 the amino acid content upon heating is challenging at present. Therefore, we direct
30 478 our focus onto the insoluble macromolecular material in the Tagish Lake meteorite.

479

480

1
2
3
4 4815 482 **4 DISCUSSION**6
7
8
9 483 **4.1 IOM in the unheated Tagish Lake sample**

10
11 484 The high abundance of aromatic material in the aqueously-altered lithology of
12
13 485 the unheated (without being treated with experimental heating) Tagish Lake meteorite
14
15 486 sample is clearly reflected in the C-XANES spectra, unbiased by the OM
16
17 487 heterogeneity in the samples (Figure 5a). The IOM in the Tagish Lake meteorite has
18
19 488 the highest aromaticity among all analyzed C1-2 chondrites (Alexander et al. 2014;
20
21 489 Cody and Alexander 2005), and is associated with elevated δD values (Pizzarello et al.
22
23 490 2001) which could be indicative of aromatization processes that have converted
24
25 491 aliphatic components into aromatic C, or an interstellar origin derived from PAHs that
26
27 492 are ubiquitous in interstellar gas (Allamandola et al. 1987). The enhanced aromaticity
28
29 493 in the more aqueously-altered lithology of the Tagish Lake meteorite is consistent
30
31 494 with the observed reduction in the abundance of sp^3 C including aliphatic (CH_n , e.g.
32
33 495 methyl, methylene, and methane) and oxygenated (CH_nO , e.g. alcohol and ether)
34
35 496 moieties, H/C ratio, and δD values correlated to the petrologic evidences of increasing
36
37 497 aqueous alteration (Alexander et al. 2014; Herd et al. 2011). These suggest that the
38
39 498 conversion of aromatic C from aliphatic C during dehydration is a more probable
40
41 499 explanation for the high aromaticity nature of the Tagish Lake OM.

42
43 500 The IOM in the least aqueously-altered lithology of the Tagish Lake meteorite
44
45 501 is more comparable to the primitive, CI-, CM- and CR-like IOM with a higher
46
47 502 aliphatic content, while that in the more aqueously-altered lithology has a lower
48
49 503 aliphatic but higher aromatic contents and thus resembles that of the mildly heated
50
51 504 CM, CV and CO chondrites (Alexander et al. 2014; Cody and Alexander 2005). In
52
53 505 this study, the Tagish Lake meteorite sample exhibits a high abundance of hydrous
54
55 506 inorganic materials (e.g., phyllosilicates), a low aliphatic organic content (Figure 5a)
56
57 507 and amino acid abundance (Table 1), which corresponds to the most extensively
58
59 508 aqueously altered Tagish Lake lithology (e.g., Alexander et al. 2014; Glavin et al.
60
61 509 2012; Herd et al. 2011; Pizzarello et al. 2001; Zolensky et al. 2002). Raman
62
63 510 spectroscopy indicates that the IOM in the Tagish Lake meteorite is composed
64
65 511 predominantly of highly-disordered C (Figure 3). While the Raman parameters of the
66
67 512 IOM show affinity to that of the primitive meteorites and clearly deviate from that of

18

1
2
3 513 the heavily heated CV and CO chondrites, we can appreciate a uniqueness in the
4 514 Tagish Lake OM as its D band parameters and I_D/I_G values do not strictly overlap with
5 515 those of the other primitive meteorites, but rather occur in regions which indicate a
6 516 higher disordered nature (Figure 3). (Matrajt et al. 2004) suggested a similarity
7 517 between the Raman spectra of the OM in the Tagish Lake meteorite and chondritic
8 518 interplanetary dust particles (IDPs). Although the OM in the unheated Tagish Lake
9 519 meteorite in our study is also shown to be highly primitive in nature, its C-XANES
10 520 and Raman spectra are distinct from those obtained for IDPs. The C-XANES spectra
11 521 of IDPs have a large absorption of aromatic, ketone and carbonyl C (e.g., Feser et al.
12 522 2003; Flynn et al. 2003; Keller et al. 2004). A substantial fraction of the IDP OM is O
13 523 substituted, and its carbonyl to aromatic C area ratio is higher than that of the Tagish
14 524 Lake OM (Figure 5), which suggests a higher thermal/aqueous processing in the latter.
15 525 The Raman C Γ_G value of the Tagish Lake OM is significantly lower than that of IDP
16 526 OM (Figure 3c,d) (Chan et al. 2017a). The more comparable Γ_G values between the
17 527 heated Tagish Lake and IDP OM are consistent with their higher O contents
18 528 compared to the unheated Tagish Lake OM.

19 529 The dehydration process experienced by the Tagish Lake meteorite was
20 530 distinctive from long-term parent body metamorphism since graphitization did not
21 531 take place, as suggested by the absence of the $1s-\sigma^*$ exciton peak in the C-XANES
22 532 spectra that would indicate highly conjugated sp^2 bonded C domains (graphene
23 533 structure) (Cody et al. 2008b). Despite the aqueous alteration-induced heating and
24 534 dehydration processes of the parent body, the heating regime would still be
25 535 considered to have occurred at “low temperatures” (<300°C) as no significant C loss
26 536 has been observed, in contrast to most hydrothermally-altered chondritic samples
27 537 (Yabuta et al. 2007). There is also a small contribution from the oxygenated
28 538 components as shown by the weak peaks around 288.5 eV in the C-XANES spectra
29 539 (Figure 5a) which indicates a minor contribution of carboxyl (O–C=O) moieties. The
30 540 contribution from these oxygenated moieties indicates the onset of a late-stage
31 541 oxidization process associated with the aqueous event, which echoes with the high
32 542 abundance of magnetite framboids and plaquettes in the Tagish Lake meteorite which
33 543 were formed via oxidation of sulfides (Zolensky et al. 2002). The consumption of O
34 544 in forming the oxides has clearly removed a significant amount of O from the
35 545 alteration fluid and limited the extent of oxidation of the organic phases.

1
2
3 546 Although the IOM has experienced a certain extent of heating associated with
4
5 547 the dehydration process, the plotted Raman parameters of the aqueously altered
6
7 548 lithology of the Tagish Lake meteorite are closer to the region of highly primitive
8
9 549 (unheated) meteorites (CMs/CRs) and clearly deviate from that of CV and CO
10 550 chondrites (Figure 3). This is because (1) the heating event was associated with a
11 551 shorter-term (<10 million years [Ma]), late-stage, low temperature (<300°C) aqueous
12 552 alteration where water acted as a thermal buffer that substituted long-term (>100 Ma),
13 553 high temperature (400–950°C) parent body thermal metamorphism (e.g., Fujiya et al.
14 554 2013; Grimm and McSween 1989; Keil 2000), (2) the aqueous event occurred at
15 555 lower temperatures, as no significant C loss was associated with the heavily-altered
16 556 lithology (Yabuta et al. 2007), and (3) the Tagish Lake IOM precursor material has a
17 557 highly primitive nature so that heating induced by short-term aqueous alteration did
18 558 not extensively anneal the OM. **Although primitive OM tends to be susceptible to
19 559 heating, heating on a short-term basis does not have the required energy to fully
20 560 transform the highly primitive into highly mature organics.**

21
22
23
24
25
26
27
28
29 561 On the basis of these observations, it is reasonable to conclude that the starting
30 562 IOM in the Tagish Lake sample prior to the heating experiments was composed of
31 563 predominantly aromatic structures with a small contribution of short- and highly-
32 564 branched aliphatic hydrocarbons and oxidized sp^2 bonded carbon, such as carboxyls
33 565 and ketones (Figure 5). NMR spectra reveal that the CO moieties (–COOR and C=O)
34 566 of the OM in the aqueously-altered Tagish Lake meteorite are not protonated, and
35 567 therefore the CO groups are ketones and not aldehydes (Cody and Alexander 2005).

36 568 **4.2 Influence of short-term heating on Raman spectral features**

37 569 The most prominent change observed for the Raman spectrum feature in
38 570 response to short-term heating is the reduction in the overall spectrum intensity. In
39 571 fact, the intensity of the Raman signal does not always reflect the OM content as it
40 572 can also be influenced by many other parameters, such as the focus of the laser.
41 573 Nevertheless, a very consistent trend has been observed for the heated samples as they
42 574 all exhibit lower Raman intensity and fluorescence background than the unheated
43 575 counterpart (Figure S5). A similar effect of heating on the fluorescence background
44 576 has been observed for the thermally-altered CM chondrites, which suggests that the
45 577 background can be influenced by the size, distribution and concentration of OM

1
2
3 578 within the sample matrix (e.g., Quirico et al. 2014). Laser-induced fluorescence
4
5 579 related to OM has been attributed to the presence of heteroatoms (e.g. N, O, and S) of
6
7 580 conjugated C bonds and aliphatic components (Busemann et al. 2007; Caro et al.
8
9 581 2006; Matrajt et al. 2004), and can be correlated to the reduction in the bulk C content
10
11 582 and IOM H/C ratios (Alexander et al. 2007; Alexander et al. 2013). Nevertheless, the
12
13 583 abundance of heteroatoms in the Tagish Lake IOM is lower than that of IDPs, as
14
15 584 suggested by the less prominent ~286.5 eV feature which can be assigned to ketones
16
17 585 (C=O), nitrile (C≡N) and/or nitrogen heterocycles (C–N=C) in the unheated Tagish
18
19 586 Lake sample (e.g., Cody et al. 2008a; Yabuta et al. 2014) (Figure 5).

20
21 587 The reduction in the fluorescence background in the heated Tagish Lake
22
23 588 sample corresponds to the decarboxylation and dehydrogenation of the aliphatic OM
24
25 589 (despite its small abundance) in the meteorite, as the OM in the heated Tagish Lake
26
27 590 meteorite gains maturity through thermal annealing by losing hydrogen and
28
29 591 heteroatoms (i.e. the hydrogenated amorphous carbons (a-C:H) fraction) to form
30
31 592 polyaromatic structures, leads to an increase in the C=C aromatic abundance and
32
33 593 reduction in the aliphatic content. Therefore, the H/C ratio of IOM is commonly used
34
35 594 as an indicator of the degree of heating in the thermally-altered carbonaceous
36
37 595 chondrites (Alexander et al. 2007; Naraoka et al. 2004). Heating of the hydrated
38
39 596 Tagish Lake sample results in the dehydration of the hydrous minerals (principally
40
41 597 saponite and serpentine) for which the released O could further oxidize the OM, while
42
43 598 further dehydrogenation could lead to the development of polycondensed aromatic
44
45 599 structures, and ultimately a reduction in the overall organic C content through
46
47 600 oxidative conversion of IOM to CO₂.

48
49 601 While the Raman data indicate that the OM in the heated Tagish Lake
50
51 602 meteorite has experienced thermal annealing by losing hydrogen and heteroatoms to
52
53 603 form polyaromatic structures, the C-XANES data do not exhibit such a consistent
54
55 604 trend between the samples that were subsampled and analyzed on different days.
56
57 605 While the C-XANES data are significantly affected by sample heterogeneity, the
58
59 606 spread of the Raman data (represented by the 1σ standard deviation of the mean,
60
61 607 $n=11-38$) suggests that the trend of the heating effect is significant and not hindered
62
63 608 by sample heterogeneity. The theoretical analytical spot size of Raman analysis (~1
64
65 609 μm) is much larger than that of C-XANES (~30 nm) and is therefore representative of

1
2
3 610 the overall organic structure and is less influenced by the OM heterogeneity at the
4
5 611 smaller scale.
6

7 612 The D band parameters show a clear trend between the OM structure and the
8
9 613 heating temperature (Figure 3a). The D band corresponds to the breathing modes in
10
11 614 rings, which is attributed to the A_{1g} mode, and is inherent in the graphite lattice. It
12
13 615 becomes observable when symmetry is broken by a crystallite edge (i.e. in-plane
14
15 616 defects). Therefore, the D band is not present in perfectly-stacked graphite or OM
16
17 617 without aromatic structure (Ferrari and Robertson 2004; Wang et al. 1990), and thus
18
19 618 the D band parameters are strong tracers of the maturity of OM that are directly
20
21 619 correlated to the presence of defects. The Γ_D value is a function of the distribution of
22
23 620 the sizes of crystalline domains, therefore as the Tagish Lake meteorite is heated, the
24
25 621 annealed OM is dominated by larger crystalline domains, which leads to a narrower D
26
27 622 band width due to reduced defects. The I_D/I_G ratio increases with heating (Figure 3b),
28
29 623 which indicates that graphitization has not been completed, as large-scale
30
31 624 graphitization would have significantly reduced I_D/I_G (Ferrari and Robertson 2000).
32
33 625 Despite the reduction in the heteroatoms and aliphatic contents, the OM is still present
34
35 626 as amorphous C and not graphitized. The rapid changes in the D band parameters and
36
37 627 the I_D/I_G ratio in response to heating up to 900°C, and the insignificant variation
38
39 628 between the 1h and 96h experiments suggest that the IOM maturation gradient
40
41 629 strongly depends on the time/temperature history, and that the Raman C parameters
42
43 630 are sensitive to short-term heating. Our observation agrees with Cody et al. (2008b) in
44
45 631 that the kinetics could be described by a log-linear behavior in response to a rapid
46
47 632 pyrolytic reaction.

48
49 633 Our experimental data also indicate that the heating experiments have led to
50
51 634 significant widening of Γ_G , and that the Γ_G value first increases and then decreases.
52
53 635 However, this trend runs counter to that for typical meteoritic organics, where
54
55 636 decreasing Γ_G is associated with increasing metamorphism (e.g., Busemann et al.
56
57 637 2007) (Figure 3c,d). Although a decrease in Γ_G ($7\text{--}10\text{ cm}^{-1}$) was associated with
58
59 638 samples that were exposed to a longer heating duration (96h), the Γ_G values are still at
60
61 639 least 14 cm^{-1} wider than the unheated samples. The challenge with Raman analysis is
62
63 640 that there is no clear functional group level correlation with Raman parameters, unlike
64
65 641 XANES analysis which can directly attribute the absorption features to a certain
66
67 642 chemical moieties. Therefore, the present data underscore the fact that the trend

1
2
3 643 observed for different Raman parameters of chondritic IOM is not rigorously tied to
4
5 644 one specific molecular structural characteristic.

6
7 645 Despite the complicated influences of varying molecular structures to the
8
9 646 Raman parameters, we can appreciate that a certain structural variation can lead to the
10
11 647 development of several trends. One confident link is that higher degrees of
12
13 648 crystallinity (ordering) favor the development of sharper bands. The G band is
14
15 649 attributed to the second E_{2g2} double degenerate in-plane vibration modes, which
16
17 650 corresponds to the C–C stretching vibration. Complete graphitic ordering into a
18
19 651 perfectly-stacked graphite results in a sharp narrow G band that corresponds to the sp^2
20
21 652 carbons of the graphene network, with the non-bonding π -orbitals only giving rise to
22
23 653 weak Van der Waals forces with minimal influences to the parallel carbon layers.
24
25 654 Therefore, a prolonged heating event, such as long-term parent body metamorphism,
26
27 655 could lead to a reduction in Γ_G via graphitic ordering, which could ultimately result in
28
29 656 very low Γ_G values once graphitization is complete. As a result, given that the OM
30
31 657 structure is well characterized, such as by determining the OM graphitization extent
32
33 658 and the abundances of oxygenated moieties, the Γ_G values can be used to distinguish
34
35 659 between short-term heating and conventional thermal metamorphism.

36
37 660 Our heating experiments provide a clear explanation for the Γ_G values
38
39 661 observed for TMCCs – their OM maturation does not strictly follow the general trend
40
41 662 observed for meteoritic IOM. For instance, with a clear dehydration history indicated
42
43 663 by the D band parameters, the G band parameter of the heated ($\geq 700^\circ\text{C}$) TMCC Y-
44
45 664 86720 plots in the zone of primitive meteorites (Busemann et al. 2007; Quirico et al.
46
47 665 2014), which required an extensive but brief heating episode following aqueous
48
49 666 alteration. The ω_D (1349 cm^{-1}) and Γ_D (245 cm^{-1}) of Y-86720 (Busemann et al. 2007)
50
51 667 would place it between the 600° and 900°C experiments on the ω_D vs Γ_D plot of
52
53 668 experimentally-heated Tagish Lake (Figure 3a). Other than the disparity between the
54
55 669 natures of the OM precursors, the difference between the trends observed for the G
56
57 670 band parameters of the OM heated under laboratory and natural processes elucidates
58
59 671 variations in their heating conditions, such as the abovementioned heating kinetics
60
61 672 and confining pressure. IOM metamorphosed naturally at depth on a chondritic parent
62
63 673 body up to kms in radius is exposed to an overburden pressure that is significantly
64
65 674 higher than that of our heating experiments (Asphaug et al. 2002). High pressure can
66
67 675 enhance the thermal transformation of organic C by reducing the temperature of

1
2
3 676 graphite formation and accelerating the graphitization process, leading to the
4 677 formation of graphite through gradual loss of hydrogen and other heteroatoms and
5 678 annealing of structural defects (Davydov et al. 2004). This justifies that short duration
6 679 heating at atmospheric pressure is not as favorable for the onset of OM graphitization
7 680 as metamorphism under high confining pressure.

681 **4.3 Absence of high order graphitic component despite heating at elevated** 682 **temperatures**

683 Fourier transform infrared (FTIR) spectroscopic analysis indicated that the
684 OM in the Tagish Lake meteorite has a significant contribution from long aliphatic
685 chains (higher CH₂/CH₃ abundance ratio) compared to other primitive meteorites
686 (Matrajt et al. 2004; Nakamura et al. 2002; Quirico et al. 2014), with a high aromatic
687 to aliphatic intensity ratio (Alexander et al. 2014; Kebukawa et al. 2011). Raman, C-
688 XANES and nuclear magnetic resonance (NMR) analyses suggested a dominant
689 aromatic constituent (Busemann et al. 2007; Cody and Alexander 2005; Matrajt et al.
690 2004; Pizzarello et al. 2001; Quirico et al. 2014).

691 No appreciable change in the aliphatic (CH_n at ~287.5 eV) moieties was
692 observed after the Tagish Lake meteorite samples were treated with experimental
693 heating. Note that aliphatic moieties are present in the Tagish Lake meteorite at a
694 small abundance and are susceptible to heating. As the aqueously-altered lithology of
695 the Tagish Lake meteorite has a small initial abundance of aliphatic hydrocarbons,
696 any further change to the aliphatic material in response to heating would be
697 unrecognizable. The aromatic moieties were progressively enriched by the loss of the
698 CO (and/or CH_n) moieties. Cleavage of hydrocarbon at elevated temperatures via
699 decomposition of CO intermediaries can form organic acids through partial oxidation,
700 which likely elucidates the high abundance of mono- and dicarboxylic acid content in
701 the Tagish Lake meteorite (Pizzarello et al. 2001). Further loss of aliphatic
702 hydrocarbon and carboxylic acids under prolonged heating would lead to total
703 oxidation, carboxylation, and decarboxylation of the hydrocarbon skeleton into CO₂.

704 While C-XANES analysis of the experimentally-heated Tagish Lake is
705 influenced by sample heterogeneity (Figure 5), our Raman data suggest that the OM
706 in the heated Tagish Lake meteorite samples exhibits lower Raman intensity and
707 fluorescence background, indicating the formation of polyaromatic structures by the

1
2
3 708 loss of hydrogen and heteroatoms (Figure 3). The widening of Γ_G in the
4
5 709 experimentally heated samples indicate an increase development in the sizes of
6
7 710 crystalline domains but graphitic ordering did not take place which would otherwise
8
9 711 have reduced the Γ_G value. This interpretation is consistent with the C-XANES
10
11 712 observation due to the absence of the graphene structure (~ 291.6 eV) that corresponds
12
13 713 to a $1s-\sigma^*$ exciton in the heated samples (Cody et al. 2008b). Although Cody et al.
14
15 714 (2008b) observed a good correlation between the intensity of the $1s-\sigma^*$ exciton and
16
17 715 Raman spectra parameter, the C-XANES data of the experimentally heated IOM
18
19 716 samples were compared with previously published Raman data (Γ_D and Γ_G) of
20
21 717 chondritic IOM (Busemann et al. 2007). Therefore it could be possible that by
22
23 718 comparing both the C-XANES and Raman data of the same laboratory heated IOM
24
25 719 would give the same trend we observed in this study.

26
27 720 As noted by Cody et al. (2008b), Murchison IOM samples flash heated for up
28
29 721 to two seconds at 600° , 1000° , and 1400°C in helium, and up to six hours at 600° ,
30
31 722 800° and 1000°C in argon, all exhibited a systematic increase in the intensity of the
32
33 723 $1s-\sigma^*$ exciton at ~ 291.6 eV. In addition to the sharp peak around 291.6 eV, a
34
35 724 pronounced broader peak at ~ 292.3 eV and graphene-like oscillations spanning out to
36
37 725 390 eV in extended X-Ray absorption fine structure (EXAFS) are also indicative of
38
39 726 the development of graphene when studying with X-ray absorption spectroscopy
40
41 727 (XAS) (G. Cody, personal communication, 2018). Although our Tagish Lake
42
43 728 meteorite samples were heated to temperatures and durations comparable to those
44
45 729 outlined in the experiments conducted by Cody et al. (2008b), the C-XANES spectra
46
47 730 of the heated Tagish Lake samples showed that OM alteration was not accompanied
48
49 731 by the development of the $1s-\sigma^*$ exciton and the OM did not transform into highly-
50
51 732 conjugated sp^2 bonded carbon domains as was clearly shown in the case of Murchison
52
53 733 IOM (Cody et al. 2008b) (Figure 5). This observation agrees with the Raman spectral
54
55 734 features: parent body metamorphism leads to the reduction in Γ_G via graphitic
56
57 735 ordering of the OM in the chondritic meteorites, however short-term heating leads to
58
59 736 the widening of Γ_G of the OM in the Tagish Lake meteorite, probably by increasing
60
737 the abundance of carboxyl moieties, but not graphitic ordering (Figure 3d). The C=O
738 stretching vibration for carboxylic acids has a strong Raman band at $1640\text{--}1685\text{ cm}^{-1}$
739 (Socrates 2001). Therefore, the presence of carboxylic acids would have widened the
740 Γ_G of the OM in the heated Tagish Lake samples.

1
2
3 741 We discuss here the two possible explanations for the Tagish Lake IOM to
4 742 behave so differently than Murchison IOM. First, the capacity for the highly altered
5 743 and aromatic-rich IOM in the Tagish Lake sample (comparable to Tagish Lake
6 744 specimens 11v and 11i) to further transform into graphene like material is limited as
7 745 there is a lack of aliphatic C to begin with (Figure 5 and Figure 6). Second, while the
8
9 746 Tagish Lake IOM is composed predominately of aromatic material, its solvent soluble
10 747 organic matter (SOM) is dominated by carboxyl and dicarboxyl compounds and a low
11 748 amino acid abundance (Pizzarello et al. 2001). In contrast, the IOM of Murchison is
12 749 composed of both aromatic and aliphatic components, but it is more enriched in
13 750 amino compounds in the soluble fraction (Martins et al. 2006; Pizzarello et al. 2001).
14 751 Therefore, heating of the OM in the Tagish Lake meteorite significantly enhances the
15 752 formation of oxygenated moieties, while heating of OM in the Murchison meteorite
16 753 mainly reduces the abundance of the aliphatic components. With a lower O/C content
17 754 in Murchison, the total loss of the aliphatic components and their conversion into
18 755 aromatics far exceeds the formation of carbonyl, which is accompanied by the loss of
19 756 electrons as H₂ (Alexander et al. 2014). Extensive dehydrogenation induces ordering
20 757 of the aromatic moieties, leading to the development of the 1s-σ* exciton in the
21 758 heated Murchison sample observed by C-XANES (Cody et al. 2008b) .

22 759 **4.4 Implications for upcoming missions visiting C-complex asteroids**

23 760 Small bodies are often loosely bound rubble-pile objects that were disrupted
24 761 into fragments before being re-accreted, and further compacted by subsequent impact
25 762 events (Okada et al. 2017b). One of the main rationales for the landing site selection
26 763 of the Hayabusa2 mission is to determine the presence of hydrated minerals by
27 764 measuring the 3 μm absorption feature with the near-IR spectrometer (NIRS3) (1.8–
28 765 3.2 μm) (Iwata et al. 2013; Okada et al. 2017a). This 3 μm feature gradually
29 766 diminishes when meteorite samples were heated to 500°C and disappears at ~700°C
30 767 in response to the dehydration of phyllosilicates (Miyamoto and Zolensky 1994;
31 768 Zolensky et al. 1994). One of the existing visible and near-infrared (VNIR)
32 769 reflectance spectra (0.5–2.5 μm) of the Cg-type (Binzel et al. 2001), near-Earth
33 770 asteroid 162173 Ryugu shows an absorption feature centered ~0.7 μm ascribed to
34 771 Fe²⁺-Fe³⁺ charge transfer in iron-bearing phyllosilicates and/or hydroxylated or
35 772 oxidized iron-bearing minerals (Vilas 2008). However, the 0.7 μm feature is evident

1
2
3 773 only in this occurrence, while the heating experiment indicated that this feature
4 774 disappears when Murchison was heated $>400^{\circ}\text{C}$ (Hiroi et al. 1994; Zolensky et al.
5 775 1994). Mid-IR spectra (5–25 μm) of Ryugu have a weak feature in the 11.4–12.5 μm
6 776 region (McAdam et al. 2015) that can be attributed to absorption bands seen from
7 777 olivine in TMCCs which indicates dehydration and dehydroxylation of phyllosilicates
8 778 (King et al. 2015a). The inconsistent occurrence of the 0.7 μm phyllosilicate feature
9 779 suggests that the surface of Ryugu is heterogeneous, and contains both hydrated and
10 780 thermally dehydrated indigenous materials (Lazzaro et al. 2013; Vilas 2008). Such
11 781 heterogeneity is a common property of main-belt C-complex asteroids (Rivkin et al.
12 782 2002), therefore it is imperative to understand the nature of organic matter and the
13 783 extent of organics lost in response to thermal processing on these C-complex asteroids,
14 784 which are the target asteroids of the OSIRIS-REx and Hayabusa2 sample return
15 785 missions.

16 786 Understanding the mineral/organic correlation on TMCCs helps to provide
17 787 guidance to the spacecraft sampling site selection in order to enhance the chances of a
18 788 successful collection of the targeted organic group. The heterogeneity of Ryugu is
19 789 best described by TMCCs, as they represent hydrated asteroids that were subsequently
20 790 heated and dehydrated. The conditions of thermal metamorphism experienced by
21 791 these meteorites are highly variable, as the heating and associated dehydration
22 792 occurred *in situ* (Nakamura 2005). Thermal metamorphism, impact heating, and solar
23 793 radiation have been proposed to be the possible heat sources, but short-term, high-
24 794 temperature impact is a more likely pathway for the Belgica group meteorites as they
25 795 appear to show no evidence of prolonged heating (Kimura and Ikeda 1992).

26 796 The chemical and bulk O isotopic compositions (Clayton and Mayeda 2001;
27 797 Engrand et al. 2001; Zolensky et al. 2002) of the matrix of the carbonate-poor
28 798 lithology of the Tagish Lake meteorite bears significant similarities to the TMCCs.
29 799 The reflectance spectrum of the Tagish Lake meteorite resembles that observed from
30 800 P- or D-type asteroids in the outer region of the main asteroid belt to a greater degree
31 801 than any other meteorite (Brown et al. 2000; Hiroi et al. 2001). The D-type asteroids
32 802 are expected to contain OM that did not experience any extensive heating and is more
33 803 primitive than those contained in any known meteorites. The Tagish Lake meteorite
34 804 has a low amino acid content (Glavin et al. 2012; Kminek et al. 2002), an extensive
35 805 suite of soluble OM that includes mono- and dicarboxylic acids, pyridine carboxylic

1
2
3 806 acids and both aliphatic and aromatic hydrocarbons (Pizzarello et al. 2001). Its IOM is
4
5 807 enriched in D and ^{15}N , and composed of predominantly aromatic structures with a
6
7 808 small contribution of short- and highly-branched aliphatic hydrocarbons and oxidized
8
9 809 sp^2 bonded carbon (Alexander et al. 2014; Herd et al. 2011; Nakamura-Messenger et
10
11 810 al. 2006; Pizzarello et al. 2001), which are indicative of their formation at low
12
13 811 temperatures and an origin of cold molecular clouds and the outer protosolar disk. The
14
15 812 highly primitive and unheated nature of the Tagish Lake meteorite makes it an ideal
16
17 813 candidate for the investigation of the effect of heating on the OM content, in contrast
18
19 814 to other chondritic OM which have already been chemically and structurally
20
21 815 thermally altered to various extents.

21 816 The results of our short-term heating experiments conducted on the more
22
23 817 hydrous lithology of the Tagish Lake meteorite imply that thermal metamorphism
24
25 818 often reduces the overall C content, particularly in the heat-sensitive SOM species.
26
27 819 Therefore, despite the short duration (up to 96h), the post-hydration local heating of
28
29 820 Ryugu could have significantly reduced the abundance and altered the primitive
30
31 821 nature of the OM, which accordingly impacts the scientific objective of the sample
32
33 822 return mission – to obtain pristine asteroidal samples that enables us to investigate the
34
35 823 diversification of organic materials through interaction with minerals and water in a
36
37 824 planetesimal (Tachibana et al. 2014; Watanabe et al. 2017).

37 825 The samples returned by the Hayabusa2 mission that are destined for SOM
38
39 826 analysis, should preferably be derived from the unheated lithology. In contrast,
40
41 827 organic analysis of the heated lithology could have been influenced by (1)
42
43 828 dehydration of phyllosilicates, (2) hydrolysis of organics at elevated temperatures by
44
45 829 the water released via phyllosilicate dehydration, (3) reduction in overall C and H/C
46
47 830 contents, (4) reduction in the aliphatic component and development of the organic C
48
49 831 into larger aromatic domains, and (5) consumption of the SOM and their
50
51 832 incorporation into the IOM structure and evolution of the IOM isotopic composition.
52
53 833 Nevertheless, serpentine without Fe^{3+} does not show the $0.7\ \mu\text{m}$ band, and not all
54
55 834 altered CM/CI meteorites exhibit this feature (McAdam et al. 2015). Therefore the
56
57 835 absence of the $0.7\ \mu\text{m}$ absorption feature is not strictly equivalent to a lack of aqueous
58
59 836 alteration or the dehydration of serpentine.
60

1
2
3 837 Several concerns regarding the proper OM interpretation are raised here. The
4
5 838 Raman spectroscopic features are controlled by the nature of the OM, the heating
6
7 839 duration and temperature. Therefore, the D band parameters of the OM that was
8
9 840 subjected to transient heating do not strictly follow the same kinetics as chondritic
10
11 841 OM that was processed by long-term thermal metamorphism (e.g. internal heating
12
13 842 from short-lived radionuclides). OM heated by transient, high temperature processes
14
15 843 on hydrous C-type asteroids cannot be described by the same D band parameters as
16
17 844 that processed by long-term heating at lower temperatures. Raman G band parameters
18
19 845 and the graphitic exciton ~291.6 eV in C-XANES can be combined to reveal the
20
21 846 heating kinetics. Therefore, the 291.6 eV absorption band in C-XANES spectra is a
22
23 847 handy cosmo-thermometer for some chondritic IOM, but it does not offer an accurate
24
25 848 description to the thermal alteration history of TMCCs, as the presence of abundant
26
27 849 hydroxylated minerals (e.g. hydroxylated phyllosilicate) and organics (e.g. carboxyls,
28
29 850 ketones) compensates for the conversion of aliphatic into aromatic components by the
30
31 851 formation of carbonyl moieties, and thus the OM does not get fully graphitized. These
32
33 852 account for the wider Γ_G in the Raman spectrum and the absence of the C-XANES
34
35 853 291.6 eV absorption band in the OM of the heated Tagish Lake meteorite samples.
36
37
38
39
40
41
42
43
44
45
46
47
48
49
50
51
52
53
54
55
56
57
58
59
60

1
2
3 854 **5 CONCLUSIONS**
4
5

6 855 We explore the effects of short-term heating on the OM in the carbonate-poor,
7
8 856 aqueously altered lithology of the Tagish Lake meteorite with Raman spectroscopy,
9
10 857 C-XANES and UPLC-FD/QToF-MS. OM maturity and graphitization is dependent
11
12 858 on the nature of the OM precursor, the heating duration and temperature, therefore the
13
14 859 Raman and C-XANES spectral features of the OM in the experimentally-heated
15
16 860 Tagish Lake meteorite samples significantly differ from that of the chondritic OM
17
18 861 such as that in Murchison which has a lower abundance of oxygenated moieties, and
19
20 862 other meteorite samples which were altered by prolonged metamorphism. Typical
21
22 863 cosmothermometers cannot be used to interpret the peak heating temperature of
23
24 864 meteorites that were altered by transient heating processes such as impact heating
25
26 865 and/or solar radiation. Nevertheless, the effect of short-term heating on the OM in the
27
28 866 Tagish Lake meteorite is well demonstrated by the distinctive Raman G band width,
29
30 867 and can be used as a guide when typical cosmothermometers cannot be applied.
31
32
33
34
35
36
37
38
39
40
41
42
43
44
45
46
47
48
49
50
51
52
53
54
55
56
57
58
59
60

869 **ACKNOWLEDGEMENTS**

870 We acknowledge Charley Roots and Jim Brook for the Tagish Lake sample.
871 This study was supported by NASA's Cosmochemistry, Emerging Worlds, and
872 Hayabusa2 Participating Scientist Programs (M.E.Z. is the PI), and the SERVII Center
873 for Lunar Science and Exploration. Q.H.S.C. acknowledges support from the NASA
874 Postdoctoral Program at the Johnson Space Center, administered by the Universities
875 Space Research Association. Y.K. is supported by the Astrobiology Center Program
876 of National Institutes of Natural Sciences (NINS) (Grant Number AB281004 and
877 AB291005). We thank George Cody for careful reviews which helped improve the
878 quality of this manuscript. We thank Aaron Burton for the use of UPLC-FD/QToF-
879 MS facility. Beamline 5.3.2.2 at the ALS is supported by the Director of the Office of
880 Science, Department of Energy under Contract No. DE-AC02-05CH11231. STXM
881 analysis in KEK (Proposal No. 2016S2-002) was supported by Ministry of Education,
882 Culture, Sports, Science and Technology (MEXT) Grant-in-Aid for Scientific
883 Research (KAKENHI) (17H06458).

884

885

886 **REFERENCES**

- 887 Akai J. 1988. Incompletely transformed serpentine-type phyllosilicates in the matrix
888 of Antarctic CM chondrites. *Geochimica et Cosmochimica Acta* 52(6): 1593-
889 1599.
- 890 Alexander C. M. O. D., Fogel M. L., Yabuta H., and Cody G. D. 2007. The origin and
891 evolution of chondrites recorded in the elemental and isotopic compositions of
892 their macromolecular organic matter. *Geochimica et Cosmochimica Acta* 71:
893 4380-4403.
- 894 Alexander C. M. O. D., Howard K. T., Bowden R., and Fogel M. L. 2013. The
895 classification of CM and CR chondrites using bulk H, C and N abundances
896 and isotopic compositions. *Geochimica et Cosmochimica Acta* 123: 244-260.
- 897 Alexander C. M. O. D., Cody G. D., Kebukawa Y., Bowden R., Fogel M. L.,
898 Kilcoyne A. L. D., Nittler L. R., and Herd C. D. K. 2014. Elemental, isotopic,
899 and structural changes in Tagish Lake insoluble organic matter produced by
900 parent body processes. *Meteoritics & Planetary Science* 49(4): 503-525.
- 901 Allamandola L. J., Sandford S. A., and Wopenka B. 1987. Interstellar Polycyclic
902 Aromatic Hydrocarbons and Carbon in Interplanetary Dust Particles and
903 Meteorites. *Science* 237(4810): 56-59.
- 904 Anders E., Hayatsu R., and Studier M. H. 1973. Organic Compounds in Meteorites
905 They may have formed in the solar nebula, by catalytic reactions of carbon
906 monoxide, hydrogen, and ammonia. *Science* 182(4114): 781-790.
- 907 Aoya M., Kouketsu Y., Endo S., Shimizu H., Mizukami T., Nakamura D., and Wallis
908 S. 2010. Extending the applicability of the Raman carbonaceous-material
909 geothermometer using data from contact metamorphic rocks. *Journal of*
910 *Metamorphic Geology* 28(9): 895-914.
- 911 Asphaug E., Ryan E. V., and Zuber M. T. 2002. Asteroid interiors. *Asteroids III* 1:
912 463-484.
- 913 Bada J. L., Miller S. L., and Zhao M. 1995. The stability of amino acids at submarine
914 hydrothermal vent temperatures. *Origins of Life and Evolution of Biospheres*
915 25(1): 111-118.
- 916 Bernard S., Beyssac O., Benzerara K., Findling N., Tzvetkov G., and Brown Jr G. E.
917 2010. XANES, Raman and XRD study of anthracene-based cokes and
918 saccharose-based chars submitted to high-temperature pyrolysis. *Carbon*
919 48(9): 2506-2516.
- 920 Beyssac O., Goffé B., Chopin C., and Rouzaud J. N. 2002. Raman spectra of
921 carbonaceous material in metasediments: a new geothermometer. *Journal of*
922 *Metamorphic Geology* 20(9): 859-871.
- 923 Binzel R. P., Harris A. W., Bus S. J., and Burbine T. H. 2001. Spectral Properties of
924 Near-Earth Objects: Palomar and IRTF Results for 48 Objects Including
925 Spacecraft Targets (9969) Braille and (10302) 1989 ML. *Icarus* 151(2): 139-
926 149.

- 1
2
3 927 Bonal L., Quirico E., Bourot-Denise M., and Montagnac G. 2006. Determination of
4 928 the petrologic type of CV3 chondrites by Raman spectroscopy of included
5 929 organic matter. *Geochimica et Cosmochimica Acta* 70(7): 1849-1863.
- 7 930 Bonal L., Bourot-Denise M., Quirico E., Montagnac G., and Lewin E. 2007. Organic
8 931 matter and metamorphic history of CO chondrites. *Geochimica et*
9 932 *Cosmochimica Acta* 71: 1605-1623.
- 11 933 Brown P. G., Hildebrand A. R., Zolensky M. E., Grady M., Clayton R. N., Mayeda T.
12 934 K., Tagliaferri E., Spalding R., MacRae N. D., Hoffman E. L., Mittlefehldt D.
13 935 W., Wacker J. F., Bird J. A., Campbell M. D., Carpenter R., Gingerich H.,
14 936 Glatiotis M., Greiner E., Mazur M. J., McCausland P. J., Plotkin H., and
15 937 Mazur T. R. 2000. The Fall, Recovery, Orbit, and Composition of the Tagish
16 938 Lake Meteorite: A New Type of Carbonaceous Chondrite. *Science* 290(5490):
17 939 320-325.
- 19 940 Burton A. S., Grunsfeld S., Elsilá J. E., Glavin D. P., and Dworkin J. P. 2014. The
20 941 effects of parent-body hydrothermal heating on amino acid abundances in CI-
21 942 like chondrites. *Polar Science* 8(3): 255-263.
- 23 943 Busemann H., Alexander M. O. D., and Nittler L. R. 2007. Characterization of
24 944 insoluble organic matter in primitive meteorites by microRaman spectroscopy.
25 945 *Meteoritics & Planetary Science* 42(7-8): 1387-1416.
- 27 946 Caro G. M. M., Matrajt G., Dartois E., Nuevo M., d'Hendecourt L., Deboffle D.,
28 947 Montagnac G., Chauvin N., Boukari C., and Du D. L. 2006. Nature and
29 948 evolution of the dominant carbonaceous matter in interplanetary dust particles:
30 949 effects of irradiation and identification with a type of amorphous carbon. *A&A*
31 950 459(1): 147-159.
- 33 951 Chan Q., Franchi I., and Wright I. 2017a Organic components in interplanetary dust
34 952 particles and their implications for the synthesis of cometary organics. In *80th*
35 953 *Annual Meeting of the Meteoritical Society 2017*, pp. 6157.
- 37 954 Chan Q. H. S., Chikaraishi Y., Takano Y., Ogawa N. O., and Ohkouchi N. 2016a.
38 955 Amino acid compositions in heated carbonaceous chondrites and their
39 956 compound-specific nitrogen isotopic ratios. *Earth, Planets and Space* 68(1): 7.
- 41 957 Chan Q. H. S., Zolensky M. E., Martinez J. E., Tsuchiyama A., and Miyake A. 2016b.
42 958 Magnetite plaquettes are naturally asymmetric materials in meteorites.
43 959 *American Mineralogist* 101(9): 2041-2050.
- 45 960 Chan Q. H. S., Zolensky M. E., Bodnar R. J., Farley C., and Cheung J. C. H. 2017b.
46 961 Investigation of organo-carbonate associations in carbonaceous chondrites by
47 962 Raman spectroscopy. *Geochimica et Cosmochimica Acta* 201: 392-409.
- 49 963 Chan Q. H. S., Zolensky M., Kebukawa Y., Fries M., Ito M., Steele A., Rahman Z.,
50 964 Nakato A., Kilcoyne A. L. D., Suga H., Takahashi Y., Takeichi Y., and Mase
51 965 K. 2018. Organic matter in extraterrestrial water-bearing salt crystals. *Science*
52 966 *Advances* 4: eaao3521.
- 54 967 Clayton R. and Mayeda T. 2001 Oxygen isotopic composition of the Tagish Lake
55 968 carbonaceous chondrite. In *Lunar and Planetary Science Conference*.
- 57 969 Clayton R. N. and Mayeda T. K. 1999. Oxygen isotope studies of carbonaceous
58 970 chondrites. *Geochimica et Cosmochimica Acta* 63(13-14): 2089-2104.

- 1
2
3 971 Cody G. D. and Alexander C. M. O. D. 2005. NMR studies of chemical structural
4 972 variation of insoluble organic matter from different carbonaceous chondrite
5 973 groups. *Geochimica et Cosmochimica Acta* 69(4): 1085-1097.
- 7 974 Cody G. D., Ade H., Alexander M. O. D., Araki T., Butterworth A., Fleckenstein H.,
8 975 Flynn G., Gilles M. K., Jacobsen C., Kilcoyne A. L. D., Messenger K.,
9 976 Sandford S. A., Tyliszczak T., Westphal A. J., Wirick S., and Yabuta H. 2008a.
10 977 Quantitative organic and light-element analysis of comet 81P/Wild 2 particles
11 978 using C-, N-, and O- μ -XANES. *Meteoritics & Planetary Science* 43(1-2): 353-
12 979 365.
- 14 980 Cody G. D., Alexander C. M. O. D., Yabuta H., Kilcoyne A. L. D., Araki T., Ade H.,
15 981 Dera P., Fogel M., Militzer B., and Mysen B. O. 2008b. Organic thermometry
16 982 for chondritic parent bodies. *Earth and Planetary Science Letters* 272(1-2):
17 983 446-455.
- 19 984 Davydov V. A., Rakhmanina A. V., Agafonov V., Narymbetov B., Boudou J. P., and
20 985 Szwarc H. 2004. Conversion of polycyclic aromatic hydrocarbons to graphite
21 986 and diamond at high pressures. *Carbon* 42(2): 261-269.
- 23 987 Derenne S. and Robert F. 2010. Model of molecular structure of the insoluble organic
24 988 matter isolated from Murchison meteorite. *Meteoritics & Planetary Science*
25 989 45(9): 1461-1475.
- 27 990 Dischler B., Bubbenzer A., and Koidl P. 1983. Bonding in hydrogenated hard carbon
28 991 studied by optical spectroscopy. *Solid State Communications* 48(2): 105-108.
- 30 992 Dry M. E. 2002. The Fischer–Tropsch process: 1950–2000. *Catalysis Today* 71(3):
31 993 227-241.
- 33 994 Engrand C., Gounelle M., Duprat J., and Zolensky M. 2001 In-situ oxygen isotopic
34 995 composition of individual minerals in Tagish Lake, a unique type 2
35 996 carbonaceous meteorite. In *Lunar and Planetary Science Conference*.
- 37 997 Ferrari A. C. and Robertson J. 2000. Interpretation of Raman spectra of disordered
38 998 and amorphous carbon. *Physical Review B* 61(20): 14095-14107.
- 40 999 Ferrari A. C. and Robertson J. 2004. Raman spectroscopy of amorphous,
41 1000 nanostructured, diamond-like carbon, and nanodiamond. *Philosophical*
42 1001 *Transactions of the Royal Society of London A: Mathematical, Physical and*
43 1002 *Engineering Sciences* 362(1824): 2477-2512.
- 45 1003 Feser M., Wirick S., Flynn G., and Keller L. 2003 Combined carbon, nitrogen, and
46 1004 oxygen XANES spectroscopy on hydrated and anhydrous interplanetary dust
47 1005 particles. In *Lunar and Planetary Science Conference*, pp. 1875, League City,
48 1006 Texas.
- 50 1007 Flynn G. J., Keller L. P., Feser M., Wirick S., and Jacobsen C. 2003. The origin of
51 1008 organic matter in the solar system: evidence from the interplanetary dust
52 1009 particles. *Geochimica et Cosmochimica Acta* 67(24): 4791-4806.
- 54 1010 Fujiya W., Sugiura N., Sano Y., and Hiyagon H. 2013. Mn–Cr ages of dolomites in
55 1011 CI chondrites and the Tagish Lake ungrouped carbonaceous chondrite. *Earth*
56 1012 *and Planetary Science Letters* 362: 130-142.

- 1
2
3 1013 Gaffey M. J., Bell J. F., and Cruikshank D. P. 1989 Reflectance spectroscopy and
4 1014 asteroid surface mineralogy. In *Asteroid II* (eds. R. P. Binzel, T. Gehrels, and
5 1015 M. S. Matthews), pp. 98-127. Univ. Arizona Press, Tucson, Arizona.
- 7 1016 Glavin D. P., Dworkin J. P., Aubrey A., Botta O., Doty III J. H., Martins Z., and Bada
8 1017 J. L. 2006. Amino acid analyses of Antarctic CM2 meteorites using liquid
9 1018 chromatography–time of flight–mass spectrometry. *Meteoritics & Planetary
10 1019 Science* 41(6): 889-902.
- 12 1020 Glavin D. P., Elsila J. E., Burton A. S., Callahan M. P., Dworkin J. P., Hilts R. W.,
13 1021 and Herd C. D. K. 2012. Unusual nonterrestrial l-proteinogenic amino acid
14 1022 excesses in the Tagish Lake meteorite. *Meteoritics & Planetary Science* 47(8):
15 1023 1347-1364.
- 17 1024 Gordon M. L., Tulumello D., Cooper G., Hitchcock A. P., Glatzel P., Mullins O. C.,
18 1025 Cramer S. P., and Bergmann U. 2003. Inner-Shell Excitation Spectroscopy of
19 1026 Fused-Ring Aromatic Molecules by Electron Energy Loss and X-ray Raman
20 1027 Techniques. *The Journal of Physical Chemistry A* 107(41): 8512-8520.
- 22 1028 Grimm R. E. and McSween H. Y. 1989. Water and the thermal evolution of
23 1029 carbonaceous chondrite parent bodies. *Icarus* 82(2): 244-280.
- 25 1030 Hayatsu R. and Anders E. 1981 Organic compounds in meteorites and their origins. In
26 1031 *Cosmo- and Geochemistry*, pp. 1-37. Springer Berlin Heidelberg.
- 28 1032 Herd C. D. K., Blinova A., Simkus D. N., Huang Y., Tarozo R., Alexander C. M. O.
29 1033 D., Gyngard F., Nittler L. R., Cody G. D., Fogel M. L., Kebukawa Y.,
30 1034 Kilcoyne A. L. D., Hilts R. W., Slater G. F., Glavin D. P., Dworkin J. P.,
31 1035 Callahan M. P., Elsila J. E., De Gregorio B. T., and Stroud R. M. 2011. Origin
32 1036 and Evolution of Prebiotic Organic Matter As Inferred from the Tagish Lake
33 1037 Meteorite. *Science* 332(6035): 1304-1307.
- 35 1038 Hiroi T., Pieters C. M., Zolensky M. E., and Lipschutz M. E. 1993. Evidence of
36 1039 Thermal Metamorphism on the C, G, B, and F Asteroids. *Science* 261(5124):
37 1040 1016-1018.
- 39 1041 Hiroi T., Peters C., Zolensky M. E., and Lipschutz P. 1994. Possible thermal
40 1042 metamorphism of the C, G, B, and F asteroids detected from their reflectance
41 1043 spectra in comparison with carbonaceous chondrites. *Proc. NIPR Symp.
42 1044 Antarctic Meteor.* 7(
- 44 1045 Hiroi T., Zolensky M. E., Pieters C. M., and Lipschutz M. E. 1996. Thermal
45 1046 metamorphism of the C, G, B, and F asteroids seen from the 0.7 μm , 3 μm ,
46 1047 and UV absorption strengths in comparison with carbonaceous chondrites.
47 1048 *Meteoritics & Planetary Science* 31(3): 321-327.
- 49 1049 Hiroi T., Zolensky M. E., and Pieters C. M. 2001. The Tagish Lake Meteorite: A
50 1050 Possible Sample from a D-Type Asteroid. *Science* 293(5538): 2234-2236.
- 52 1051 Homma Y., Kouketsu Y., Kagi H., Mikouchi T., and Yabuta H. 2015. Raman
53 1052 spectroscopic thermometry of carbonaceous material in chondrites: four-band
54 1053 fitting analysis and expansion of lower temperature limit. *Journal of
55 1054 Mineralogical and Petrological Sciences* 110(6): 276-282.
- 57 1055 Ikeda Y. 1991. Petrology and mineralogy of the Yamato-82162 chondrite (CI). *Proc.
58 1056 NIPR Symp. Antarctic Meteor.* 4(

- 1
2
3 1057 Ikeda Y. 1992. An overview of the research consortium, “Antarctic carbonaceous
4 1058 chondrites with CI affinities, Yamato-86720, Yamato-82162 and Belgica-
5 1059 7904”. Proc. NIPR Symp. Antarctic Meteor. 5(
6
7 1060 Iwata T., Kitazato K., Abe M., Ohtake M., Matsuura S., Tsumura K., Hirata N.,
8 1061 Honda C., Takagi Y., and Nakauchi Y. 2013 Results of the critical design for
9 1062 nirs3: the near infrared spectrometer on Hayabusa-2. In *Lunar and Planetary*
10 1063 *Science Conference*, pp. 1908.
11
12 1064 Kebukawa Y., Alexander C. M. O. D., and Cody G. D. 2011. Compositional diversity
13 1065 in insoluble organic matter in type 1, 2 and 3 chondrites as detected by
14 1066 infrared spectroscopy. *Geochimica et Cosmochimica Acta* 75(12): 3530-3541.
15
16 1067 Kebukawa Y., Zolensky M. E., Chan Q. H. S., Nagao K., Kilcoyne A. L. D., Bodnar
17 1068 R. J., Farley C., Rahman Z., Le L., and Cody G. D. 2017. Characterization of
18 1069 carbonaceous matter in xenolithic clasts from the Sharps (H3.4) meteorite:
19 1070 Constraints on the origin and thermal processing. *Geochimica et*
20 1071 *Cosmochimica Acta* 196: 74-101.
21
22 1072 Keil K. 2000. Thermal alteration of asteroids: evidence from meteorites. *Planetary*
23 1073 *and Space Science* 48(10): 887-903.
24
25 1074 Keller L. P., Messenger S., Flynn G. J., Clemett S., Wirick S., and Jacobsen C. 2004.
26 1075 The nature of molecular cloud material in interplanetary dust. *Geochimica et*
27 1076 *Cosmochimica Acta* 68(11): 2577-2589.
28
29 1077 Kilcoyne A. L. D., Tyliszczak T., Steele W. F., Fakra S., Hitchcock P., Franck K.,
30 1078 Anderson E., Harteneck B., Rightor E. G., Mitchell G. E., Hitchcock A. P.,
31 1079 Yang L., Warwick T., and Ade H. 2003. Interferometer-controlled scanning
32 1080 transmission X-ray microscopes at the Advanced Light Source. *Journal of*
33 1081 *Synchrotron Radiation* 10(2): 125-136.
34
35 1082 Kimura M. and Ikeda Y. 1992. Mineralogy and petrology of an unusual Belgica-7904
36 1083 carbonaceous chondrites: genetic relationships among the components. Proc.
37 1084 NIPR Symp. Antarctic Meteor. 5(
38
39 1085 King A., Solomon J., Schofield P., and Russell S. 2015a. Characterising the CI and
40 1086 CI-like carbonaceous chondrites using thermogravimetric analysis and
41 1087 infrared spectroscopy. *Earth, Planets and Space* 67(1): 1-12.
42
43 1088 King A. J., Schofield P. F., Howard K. T., and Russell S. S. 2015b. Modal mineralogy
44 1089 of CI and CI-like chondrites by X-ray diffraction. *Geochimica et*
45 1090 *Cosmochimica Acta* 165: 148-160.
46
47 1091 Kitadai N. 2016. Predicting Thermodynamic Behaviors of Non-Protein Amino Acids
48 1092 as a Function of Temperature and pH. *Origins of Life and Evolution of*
49 1093 *Biospheres* 46(1): 3-18.
50
51 1094 Kminek G., Botta O., Glavin D. P., and Bada J. L. 2002. Amino acids in the Tagish
52 1095 Lake meteorite. *Meteoritics & Planetary Science* 37(5): 697-701.
53
54 1096 Kouketsu Y., Mizukami T., Mori H., Endo S., Aoya M., Hara H., Nakamura D., and
55 1097 Wallis S. 2014. A new approach to develop the Raman carbonaceous material
56 1098 geothermometer for low-grade metamorphism using peak width. *Island Arc*
57 1099 23(1): 33-50.
58
59
60

- 1
2
3 1100 Lancet M. S. and Anders E. 1970. Carbon Isotope Fractionation in the Fischer-
4 1101 Tropsch Synthesis and in Meteorites. *Science* 170(3961): 980-982.
5
6 1102 Lazzaro D., Barucci M. A., Perna D., Jasmim F. L., Yoshikawa M., and Carvano J. M.
7 1103 F. 2013. Rotational spectra of (162173) 1999 JU3, the target of the Hayabusa2
8 1104 mission. *Astronomy & Astrophysics* 549: L2.
9
10 1105 Le Guillou C., Bernard S., Brearley A. J., and Remusat L. 2014. Evolution of organic
11 1106 matter in Orgueil, Murchison and Renazzo during parent body aqueous
12 1107 alteration: In situ investigations. *Geochimica et Cosmochimica Acta* 131: 368-
13 1108 392.
14
15 1109 Lessard R., Cuny J., Cooper G., and Hitchcock A. P. 2007. Inner-shell excitation of
16 1110 gas phase carbonates and α,γ -dicarbonyl compounds. *Chemical Physics*
17 1111 331(2): 289-303.
18
19 1112 Martins Z., Watson J. S., Sephton M. A., Botta O., Ehrenfreund P., and Gilmour I.
20 1113 2006. Free dicarboxylic and aromatic acids in the carbonaceous chondrites
21 1114 Murchison and Orgueil. *Meteoritics & Planetary Science* 41(7): 1073-1080.
22
23 1115 Matrajt G., Borg J., Raynal P. I., Djouadi Z., d'Hendecourt L., Flynn G., and Deboffle
24 1116 D. 2004. FTIR and Raman analyses of the Tagish Lake meteorite:
25 1117 Relationship with the aliphatic hydrocarbons observed
26 1118 in the Diffuse Interstellar Medium. *A&A* 416(3): 983-990.
27
28 1119 McAdam M. M., Sunshine J. M., Howard K. T., and McCoy T. M. 2015. Aqueous
29 1120 alteration on asteroids: Linking the mineralogy and spectroscopy of CM and
30 1121 CI chondrites. *Icarus* 245: 320-332.
31
32 1122 Miyamoto M. and Zolensky M. E. 1994. Infrared diffuse reflectance spectra of
33 1123 carbonaceous chondrites: Amount of hydrous minerals. *Meteoritics* 29(6):
34 1124 849-853.
35
36 1125 Nakamura-Messenger K., Messenger S., Keller L. P., Clemett S. J., and Zolensky M.
37 1126 E. 2006. Organic Globules in the Tagish Lake Meteorite: Remnants of the
38 1127 Protosolar Disk. *Science* 314(5804): 1439-1442.
39
40 1128 Nakamura K., Zolensky M. E., Tomita S., Nakashima S., and Tomeoka K. 2002.
41 1129 Hollow organic globules in the Tagish Lake meteorite as possible products of
42 1130 primitive organic reactions. *International Journal of Astrobiology* 1(03): 179-
43 1131 189.
44
45 1132 Nakamura T. 2005. Post-hydration thermal metamorphism of carbonaceous
46 1133 chondrites. *J. Mineral. Petrol. Sci.* 100(
47
48 1134 Nakato A., Nakamura T., Kitajima F., and Noguchi T. 2008. Evaluation of
49 1135 dehydration mechanism during heating of hydrous asteroids based on
50 1136 mineralogical and chemical analysis of naturally and experimentally heated
51 1137 CM chondrites. *Earth, Planets and Space* 60(8): 855-864.
52
53 1138 Nakato A., Chan Q., Nakamura T., Kebukawa Y., and Zolensky M. 2016 Mineralogy
54 1139 of Experimentally Heated Tagish Lake. In *Lunar and Planetary Science*
55 1140 *Conference*, The Woodlands, TX; United States.
56
57 1141 Naraoka H., Mita H., Komiya M., Yoneda S., Kojima H., and Shimoyama A. 2004. A
58 1142 chemical sequence of macromolecular organic matter in the CM chondrites.
59 1143 *Meteoritics & Planetary Science* 39(3): 401-406.
60

- 1
2
3 1144 Okada T., Binzel R. P., Connolly H. C., Yada T., and Ohtsuki K. 2017a. Special issue
4 1145 “Science of solar system materials examined from Hayabusa and future
5 1146 missions (II)”. *Earth, Planets and Space* 69(1): 31.
- 7 1147 Okada T., Fukuhara T., Tanaka S., Taguchi M., Imamura T., Arai T., Senshu H.,
8 1148 Ogawa Y., Demura H., Kitazato K., Nakamura R., Kouyama T., Sekiguchi T.,
9 1149 Hasegawa S., Matsunaga T., Wada T., Takita J., Sakatani N., Horikawa Y.,
10 1150 Endo K., Helbert J., Müller T. G., and Hagermann A. 2017b. Thermal Infrared
11 1151 Imaging Experiments of C-Type Asteroid 162173 Ryugu on Hayabusa2.
12 1152 *Space Science Reviews* 208(1): 255-286.
- 14 1153 Pearson V. K., Sephton M. A., Franchi I. A., Gibson J. M., and Gilmour I. 2006.
15 1154 Carbon and nitrogen in carbonaceous chondrites: Elemental abundances and
16 1155 stable isotopic compositions. *Meteoritics & Planetary Science* 41(12): 1899-
17 1156 1918.
- 19 1157 Pietrucci F., Aponte J. C., Starr R., Pérez-Villa A., Elsilá J. E., Dworkin J. P., and
20 1158 Saitta A. M. 2018. Hydrothermal Decomposition of Amino Acids and Origins
21 1159 of Prebiotic Meteoritic Organic Compounds. *ACS Earth and Space Chemistry*.
- 23 1160 Pizzarello S., Huang Y., Becker L., Poreda R. J., Nieman R. A., Cooper G., and
24 1161 Williams M. 2001. The Organic Content of the Tagish Lake Meteorite.
25 1162 *Science* 293(5538): 2236-2239.
- 27 1163 Pizzarello S. 2012. Catalytic syntheses of amino acids and their significance for
28 1164 nebular and planetary chemistry. *Meteoritics & Planetary Science* 47(8): 1291-
29 1165 1296.
- 31 1166 Quirico E., Raynal P.-I., and Bourot-Denise M. 2003. Metamorphic grade of organic
32 1167 matter in six unequilibrated ordinary chondrites. *Meteoritics & Planetary
33 1168 Science* 38(6): 795-811.
- 35 1169 Quirico E., Orthous-Daunay F.-R., Beck P., Bonal L., Brunetto R., Dartois E., Pino T.,
36 1170 Montagnac G., Rouzaud J.-N., Engrand C., and Duprat J. 2014. Origin of
37 1171 insoluble organic matter in type 1 and 2 chondrites: New clues, new questions.
38 1172 *Geochimica et Cosmochimica Acta* 136: 80-99.
- 40 1173 Ratcliff M. A., Medley E. E., and Simmonds P. G. 1974. Pyrolysis of amino acids.
41 1174 Mechanistic considerations. *The Journal of Organic Chemistry* 39(11): 1481-
42 1175 1490.
- 44 1176 Rivkin A., Howell E., Vilas F., and Lebofsky L. 2002. Hydrated minerals on
45 1177 asteroids: The astronomical record. *Asteroids III* 1: 235-253.
- 47 1178 Socrates G. 2001 *Infrared and Raman Characteristic Group Frequencies: Tables and
48 1179 Charts*. John Wiley & Sons. pp. 347.
- 50 1180 Tachibana S., Abe M., Arakawa M., Fujimoto M., Iijima Y., Ishiguro M., Kitazato K.,
51 1181 Kobayashi N., Namiki N., Okada T., Okazaki R., Sawada H., Sugita S.,
52 1182 Takano Y., Tanaka S., Watanabe S., Yoshikawa M., Kuninaka H., and The
53 1183 Hayabusa2 Project T. 2014. Hayabusa2: Scientific importance of samples
54 1184 returned from C-type near-Earth asteroid (162173) 1999 JU₃. *Geochemical
55 1185 Journal* 48(6): 571-587.
- 57 1186 Takeichi Y., Inami N., Suga H., Miyamoto C., Ueno T., Mase K., Takahashi Y., and
58 1187 Ono K. 2016. Design and performance of a compact scanning transmission X-

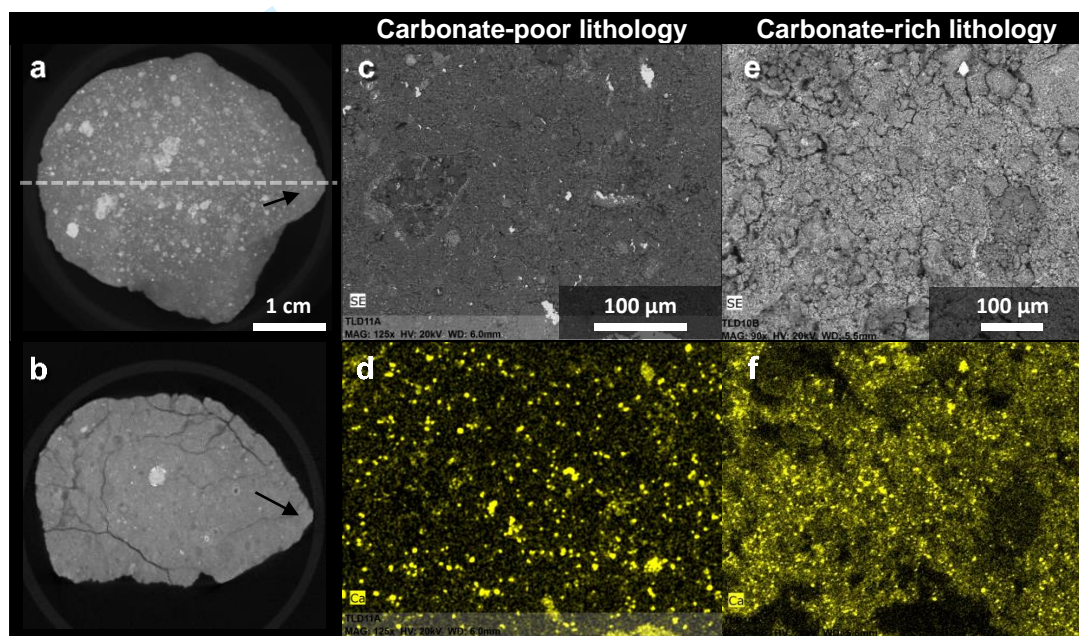
- 1
2
3 1188 ray microscope at the Photon Factory. Review of Scientific Instruments 87(1):
4 1189 013704.
- 6 1190 Tomeoka K., Kojima H., and Yanai K. 1989a. Yamato-82162: a new kind of CI
7 1191 carbonaceous chondrite from Antarctica. Proc. NIPR Symp. Antarctic Meteor.
8 1192 2(
9
- 11 1193 Tomeoka K., Kojima H., and Yanai K. 1989b. Yamato-86720: A CM carbonaceous
11 1194 chondrite having experienced extensive aqueous alteration and thermal
12 1195 metamorphism. Proc. NIPR Symp. Antarctic Meteor. 2(
13
- 14 1196 Tonui E., Zolensky M., Hiroi T., Nakamura T., Lipschutz M. E., Wang M.-S., and
15 1197 Okudaira K. 2014. Petrographic, chemical and spectroscopic evidence for
16 1198 thermal metamorphism in carbonaceous chondrites I: CI and CM chondrites.
17 1199 *Geochimica et Cosmochimica Acta* 126: 284-306.
- 19 1200 Tuinstra F. and Koenig J. L. 1970a. Characterization of Graphite Fiber Surfaces with
20 1201 Raman Spectroscopy. *Journal of Composite Materials* 4(4): 492-499.
- 22 1202 Tuinstra F. and Koenig J. L. 1970b. Raman Spectrum of Graphite. *The Journal of*
23 1203 *Chemical Physics* 53(3): 1126-1130.
- 24 1204 Vilas F. 2008. Spectral Characteristics of Hayabusa 2 Near-Earth Asteroid Targets
25 1205 162173 1999 JU3 and 2001 QC34. *The Astronomical Journal* 135(4): 1101.
- 27 1206 Wang Y., Alsmeyer D. C., and McCreery R. L. 1990. Raman spectroscopy of carbon
28 1207 materials: structural basis of observed spectra. *Chemistry of Materials* 2(5):
29 1208 557-563.
- 31 1209 Watanabe S.-i., Tsuda Y., Yoshikawa M., Tanaka S., Saiki T., and Nakazawa S. 2017.
32 1210 Hayabusa2 Mission Overview. *Space Science Reviews* 208(1): 3-16.
- 34 1211 Yabuta H., Williams L. B., Cody G. D., Alexander C. M. O. D., and Pizzarello S.
35 1212 2007. The insoluble carbonaceous material of CM chondrites: A possible
36 1213 source of discrete organic compounds under hydrothermal conditions.
37 1214 *Meteoritics & Planetary Science* 42(1): 37-48.
- 39 1215 Yabuta H., Alexander C. M. O. D., Fogel M. L., Kilcoyne A. L. D., and Cody G. D.
40 1216 2010. A molecular and isotopic study of the macromolecular organic matter of
41 1217 the ungrouped C2 WIS 91600 and its relationship to Tagish Lake and PCA
42 1218 91008. *Meteoritics & Planetary Science* 45(9): 1446-1460.
- 44 1219 Yabuta H., Uesugi M., Naraoka H., Ito M., Kilcoyne A., Sandford S., Kitajima F.,
45 1220 Mita H., Takano Y., Yada T., Karouji Y., Ishibashi Y., Okada T., and Abe M.
46 1221 2014. X-ray absorption near edge structure spectroscopic study of Hayabusa
47 1222 category 3 carbonaceous particles. *Earth, Planets and Space* 66(1): 1-8.
- 49 1223 Yoshino D., Hayatsu K., and Anders E. 1971. Origin of organic matter in early solar
50 1224 system—III. Amino acids: Catalytic synthesis. *Geochimica et Cosmochimica*
51 1225 *Acta* 35(9): 927-938.
- 53 1226 Zolensky M., Lipschutz M., and Hiroi T. 1994 Mineralogy of artificially heated
54 1227 carbonaceous chondrites. In *Lunar and Planetary Science Conference*, pp.
55 1228 1567-1568.
- 57 1229 Zolensky M. E., Nakamura K., Gounelle M., Mikouchi T., Kasama T., Tachikawa O.,
58 1230 and Tonui E. 2002. Mineralogy of Tagish Lake: An ungrouped type 2
59 1231 carbonaceous chondrite. *Meteoritics & Planetary Science* 37(5): 737-761.

1
2
3 1232
4
5 1233
6
7 1234
8
9
10
11
12
13
14
15
16
17
18
19
20
21
22
23
24
25
26
27
28
29
30
31
32
33
34
35
36
37
38
39
40
41
42
43
44
45
46
47
48
49
50
51
52
53
54
55
56
57
58
59
60

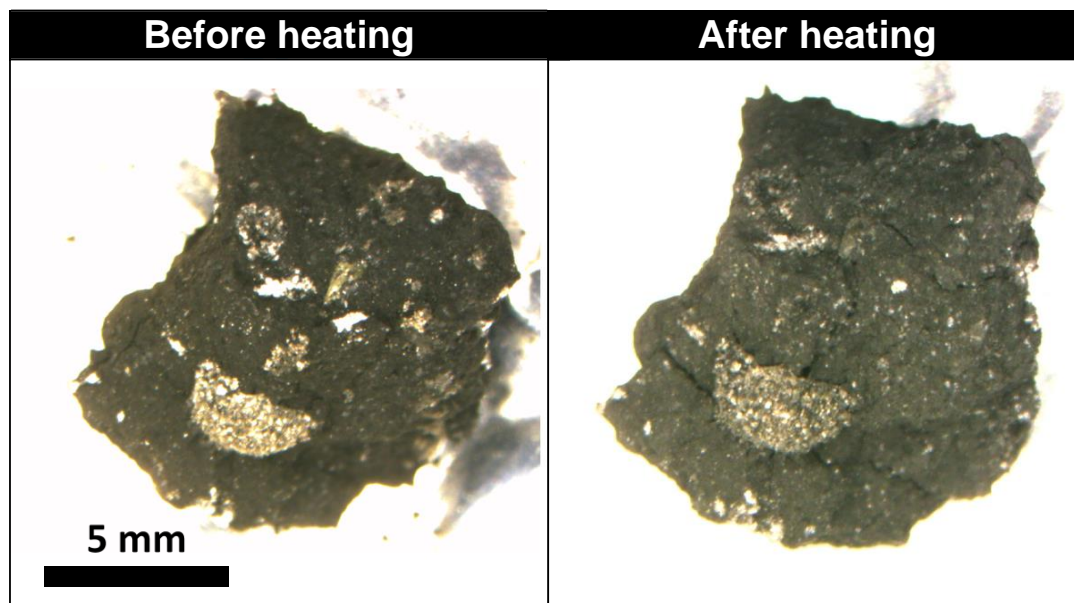
For Peer Review Only

1
2
3 1235 **FIGURES AND FIGURE CAPTIONS**
4
5

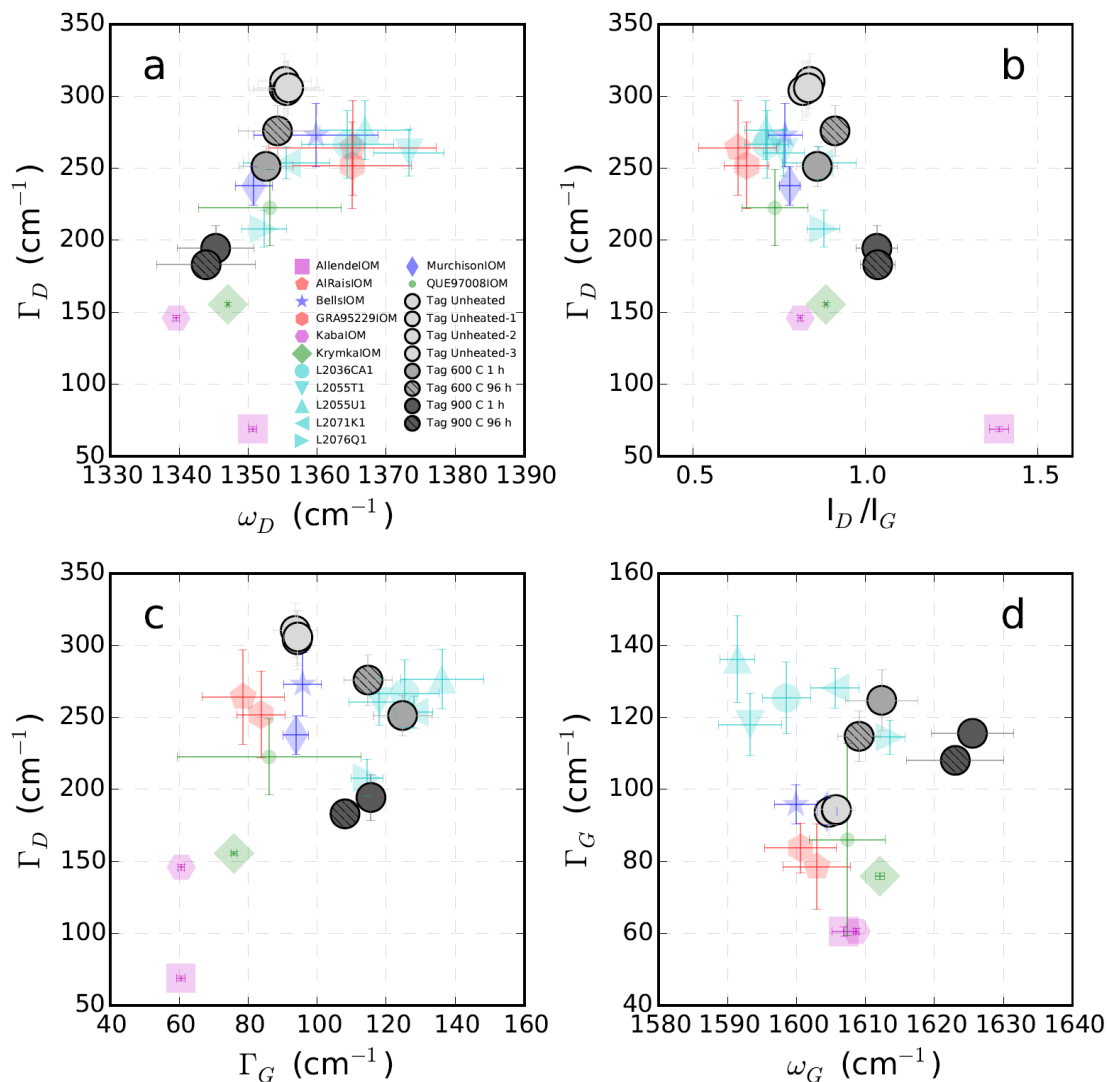
6 1236 Figure 1. (a) 3D rendering of the Tagish Lake meteorite samples produced from
7 1237 XRCT. The arrow shows the area of the carbonate-poor lithology. (b) A slice image
8 1238 of Tagish Lake sample taken at the dashed line in (a). SE images (c,e) and EDX Ca
9 1239 X-ray maps (d,f) of the carbonate-rich (right) and carbonate-poor (middle) lithologies
10 1240 of the Tagish Lake meteorite, obtained by SEM analysis. All EDX elemental maps of
11 1241 the carbonate-poor lithology are shown in Figure S1.
12
13
14
15
16



1
2
3 1244 Figure 2. Optical photos of the Tagish Lake meteorite sample before and after the
4 heating experiment at 900°C for 96h. The sample shows significant weight loss
5 (~20%) upon heating which indicates the dehydration of phyllosilicates. Common
6 mineral phases observed in the matrix of the unheated carbonate-poor lithology of the
7 Tagish Lake meteorite such as phyllosilicates, magnetite and Fe-Ni sulfides were
8 converted into anhydrous silicates, Fe-Ni metal and troilite via dehydration and
9 reduction.
10
11
12
13
14
15

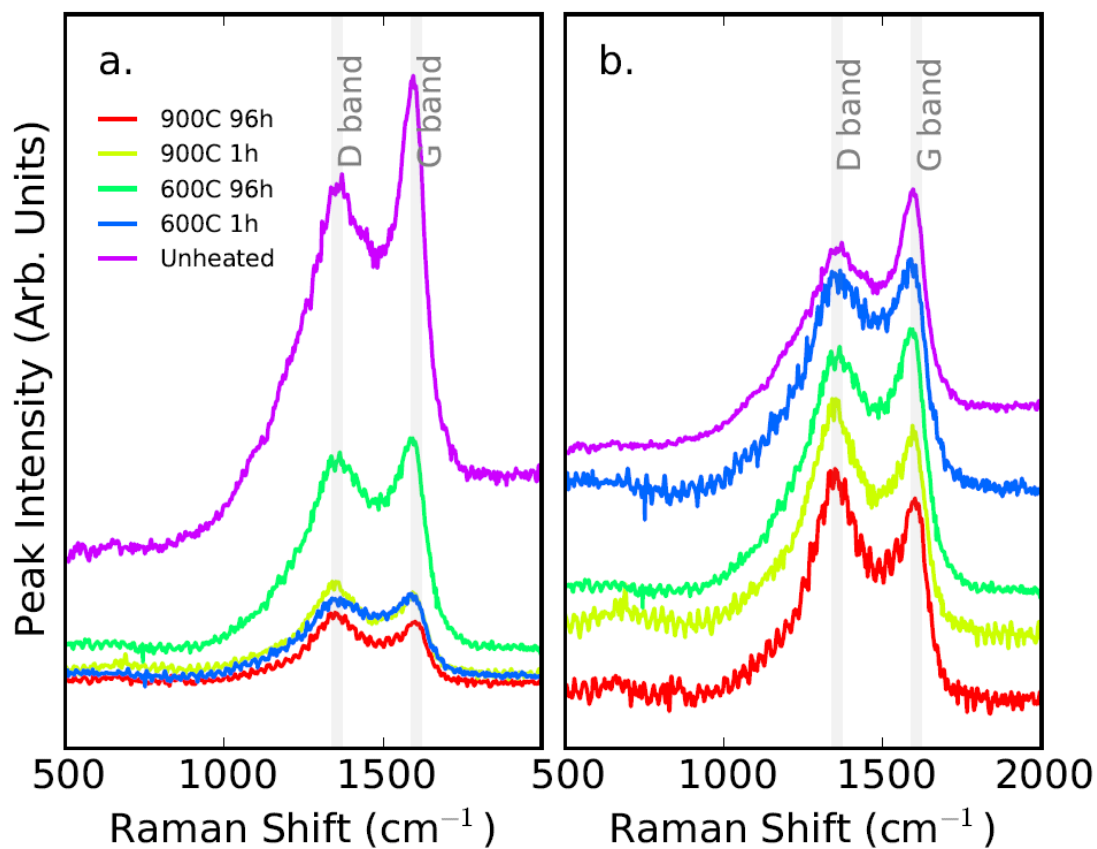


1252 Figure 3. Comparison of the C Raman band parameters of the OM in the heating-
 1253 experimental products of the Tagish Lake meteorite to the OM in chondrites and IDPs.
 1254 Data of the chondrites and IDPs were obtained from Chan et al. (2017a).
 1255 Uncertainties are 1 σ standard deviation of the mean.

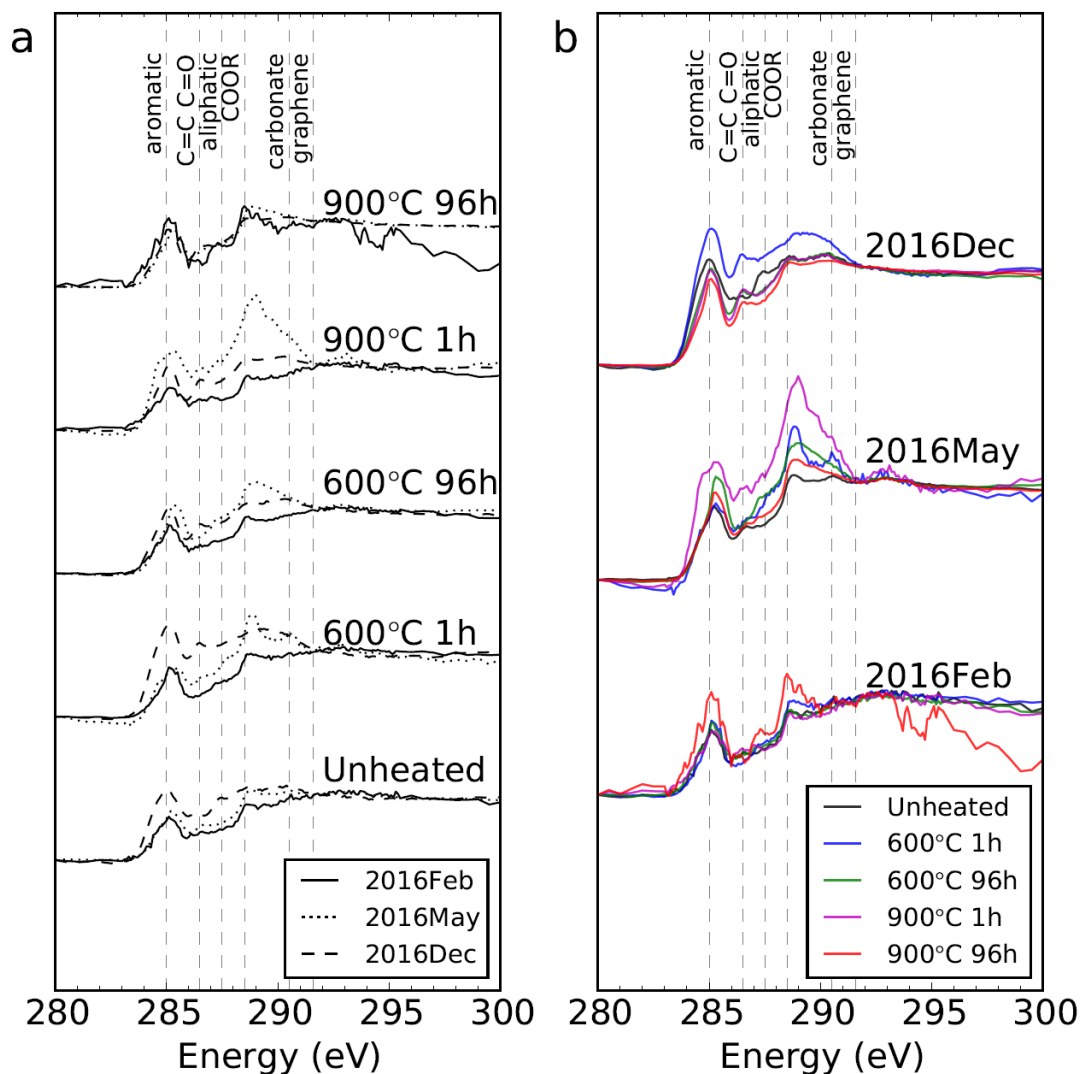


1256
1257

1
2
3 1258 Figure 4. (a) Selected representative raw Raman spectra of the unheated and heated
4 Tagish Lake meteorite samples. (b) The same Raman spectra which have been
5 1259 Tagish Lake meteorite samples. (b) The same Raman spectra which have been
6 normalized with respect to the maximum intensity within the spectral range 1580–
7 1260 normalized with respect to the maximum intensity within the spectral range 1580–
8 1261 1630 cm^{-1} . The spectra have been offset vertically to enhance readability.



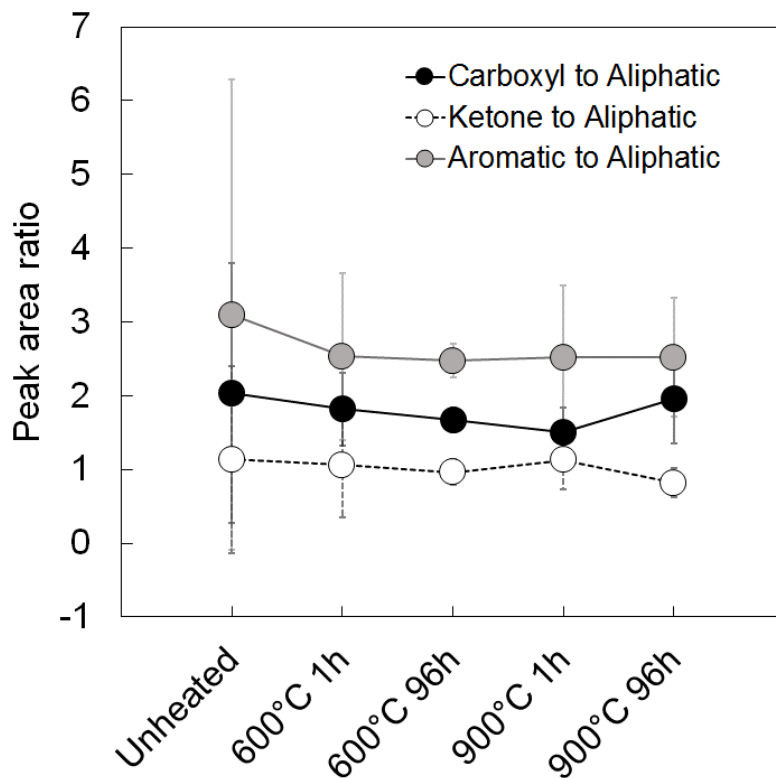
1
2
3 1264 Figure 5. C-XANES spectra of different FIB sections from the Tagish Lake meteorite
4 samples before and after heating to 600° and 900°C for 1 and 96h, obtained on
5 1265 separate dates. The spectra are presented in two subplots: (a) spectra are grouped
6 1266 according to the heating conditions, and (b) spectra are grouped according to different
7 1267 analytical dates. The spectra have been offset vertically to enhance readability.
8 1268



1269

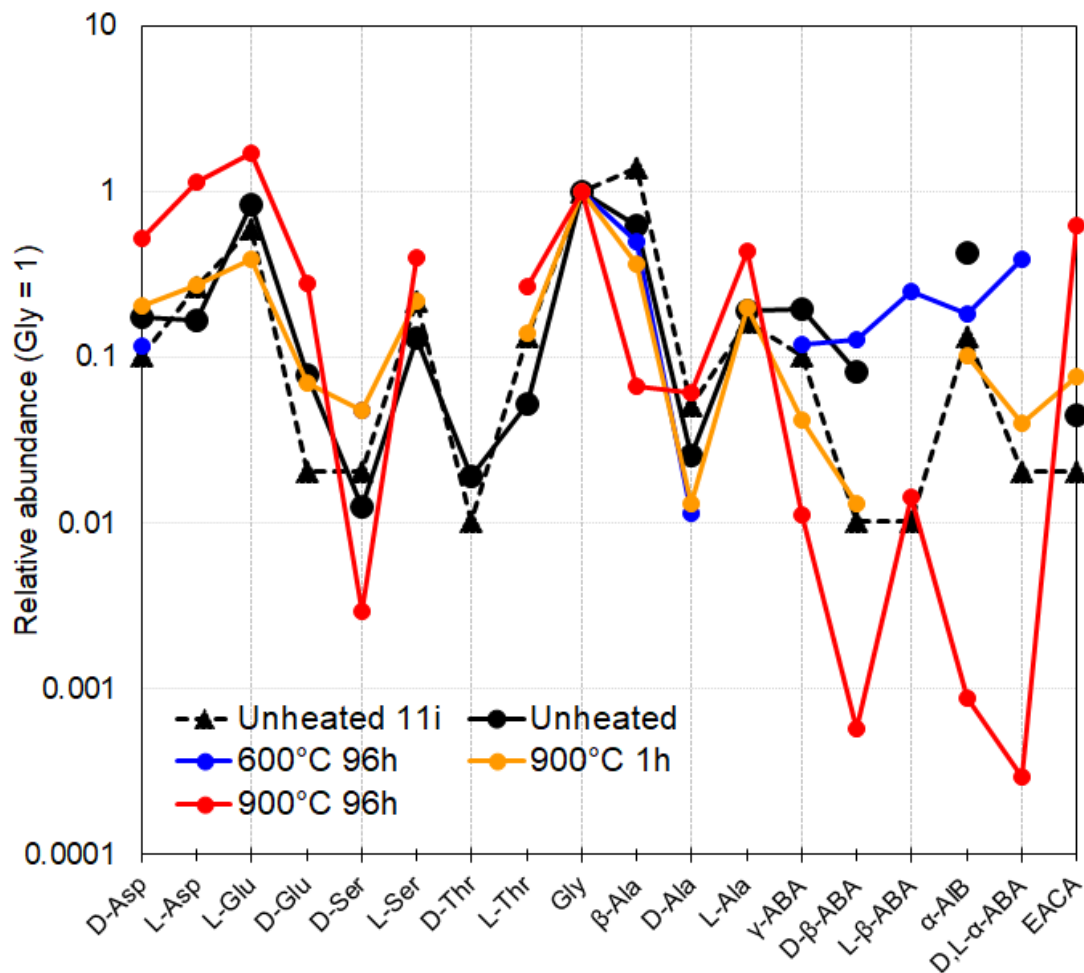
1270

1
2
3 1271 Figure 6. Comparison of the C-XANES peak area ratios between the IOM in Tagish
4 1272 Lake samples at different experimental heating conditions. Error bars are the standard
5 1273 deviation of the mean of the three FIB sections prepared for each experimental
6 1274 condition, which represent sample heterogeneity. The C-XANES raw spectra were
7 1275 first normalized to the total amount of C (absorption from 283-292 eV). The spectra
8 1276 were then fitted with an arctangent function to model the absorption edge (the center
9 1277 position, amplitude and width of the arctangent function are fixed to 291.5 eV, 1.0,
10 1278 and 0.4 eV, respectively) (Bernard et al. 2010) and Gaussian functions with a fixed
11 1279 energy position and a constant width (0.4 eV below 295 eV and 2 eV above).



1280

1
2
3 1281 Figure 7. The relative amino acid abundances (relative to glycine) in the unheated and
4 1282 experimentally-heated Tagish Lake meteorite samples. Data of the aqueously altered
5 1283 lithology (#11i) of the Tagish Lake meteorite from Glavin et al. (2012) are shown
6 1284 here for comparison.



1285
1286

1287 **TABLE AND TABLE CAPTIONS**

1288 Table 1. Summary of the average abundances (in ppb) of identified amino acids in the
 1289 blank-corrected 6 M HCl-hydrolyzed (total) hot-water extracts of the unheated and
 1290 experimentally-heated Tagish Lake meteorite measured by UPLC-FD/QToF-MS.

	Unheated	600°C 96h	900°C 1h	900°C 96h	Unheated 11i ^a
D-Asp	3.8 ± 3.5	5.7 ± 2.9	6.3 ± 5.3	61.3 ± 49	<1
L-Asp	3.7 ± 0.3	n.d.	8.5 ± 0.6	132.9 ± 13.3	2.6 ± 0.5
L-Glu	18.3 ± 9.1	n.d.	12.2 ± 6.8	198.5 ± 108	<5.8
D-Glu	1.7 ± 0.8	n.d.	2.2 ± 2.3	32.2 ± 16.5	0.2 ± 1.6
D-Ser	0.3 ± 0.2	2.3 ± 2.4	1.5 ± 2	<0.7	<0.2
L-Ser	2.9 ± 0.5	n.d.	6.8 ± 1.6	46.9 ± 17.7	2.1 ± 0.9
D-Thr	<0.8	n.d.	n.d.	n.d.	<0.1
L-Thr	1.2 ± 0.1	n.d.	4.3 ± 3	30.9 ± 6.3	1.3 ± 0.4
Gly	21.9 ± 15.4	48.9 ± 47.3	31.1 ± 18.7	116.6 ± 114.1	9.7 ± 4.2
β-Ala	13.8 ± 1.3	24.4 ± 8	11.4 ± 4.1	7.8 ± 5.7	13.5 ± 0.7
D-Ala	<1.1	<1.1	<0.8	7.1 ± 0	<0.5
L-Ala	4.2 ± 0.3	n.d.	6.2 ± 0.2	50.3 ± 17.7	<1.6
γ-ABA	4.3 ± 2.1	5.8 ± 3.7	1.3 ± 0.5	1.3 ± 0.9	1 ± 0.5
D-β-ABA	<3.6	6.3 ± 8.1	0.4 ± 0.2	<0.1	<0.1
L-β-ABA	n.d.	<24.2	n.d.	1.7 ± 1.6	<0.1
α-AIB	9.3 ± 11.5	<17.6	3.1 ± 2	<0.2	1.3 ± 0.2
D,L-α-ABA	n.d.	<37.8	1.2 ± 1.7	<0.1	<0.2
EACA	<2	n.d.	2.4 ± 0.2	72.3 ± 41.5	<0.2
Total	~89.1	~133.8	~99.4	~760.3	~41.5
Total D-amino acids	~8.5	~8.3	~33.8	~41	~12.1

1291 ^a The amino acids in the acid hydrolyzed hot-water extract of the aqueously altered
 1292 lithology (#11i) of the Tagish Lake meteorite given by (Glavin et al. 2012) are shown
 1293 here for comparison.

1294 **Abbreviations; Asp: aspartic acid, Glu: glutamic acid, Ser: serine, Thr: threonine, Gly:**
 1295 **glycine, Ala: alanine, ABA: aminobutyric acid, AIB: aminoisobutyric acid, EACA: ε-**
 1296 **amino-*n*-caproic acid.**

SUPPLEMENTARY MATERIALS**for****Heating experiments of the Tagish Lake meteorite: investigation of the effects of short-term heating on chondritic organics**

Queenie H. S. Chan^{1*†}, Aiko Nakato², Yoko Kebukawa³, Michael E. Zolensky¹, Tomoki Nakamura⁴, Jessica A. Maisano⁵, Matthew W. Colbert⁵, James E. Martinez⁶, A.L. David Kilcoyne⁷, Hiroki Suga⁸, Yoshio Takahashi⁹, Yasuo Takeichi^{10,11}, Kazuhiko Mase^{10,11} and Ian P. Wright¹

*Corresponding author: Queenie H. S. Chan (E-mail: Queenie.Chan@open.ac.uk; Telephone: +1 (585) 653-6144).

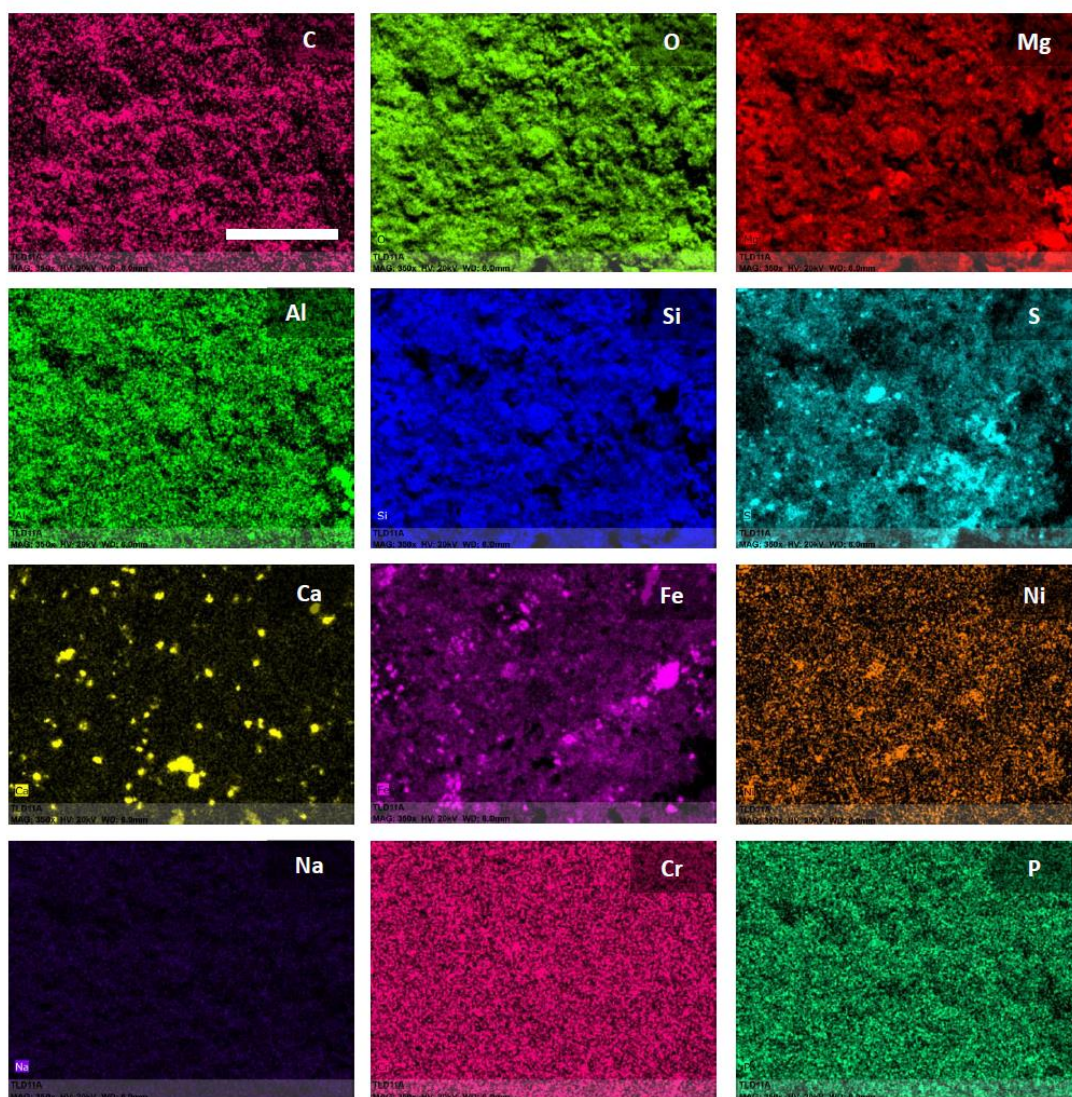
This file includes:

Figures S1 to S5

Tables S1

Movies S1 to S2

Figure S1. EDX X-ray maps of the carbonate-poor lithology. Scale bar is 100 μ m.



Only

Figure S2. Peak-fitting results obtained with LBWF curve-fitting model in the first-order region ($1000\text{--}1800\text{ cm}^{-1}$) of the unheated Tagish Lake meteorite sample showing (top) the linear-background-corrected data (\bullet), the fitted spectrum (black smooth solid line) and the decomposed D (green dashed line) and G (red dashed line) bands, (middle) the raw spectrum, and (bottom) the spectral fitting residue.

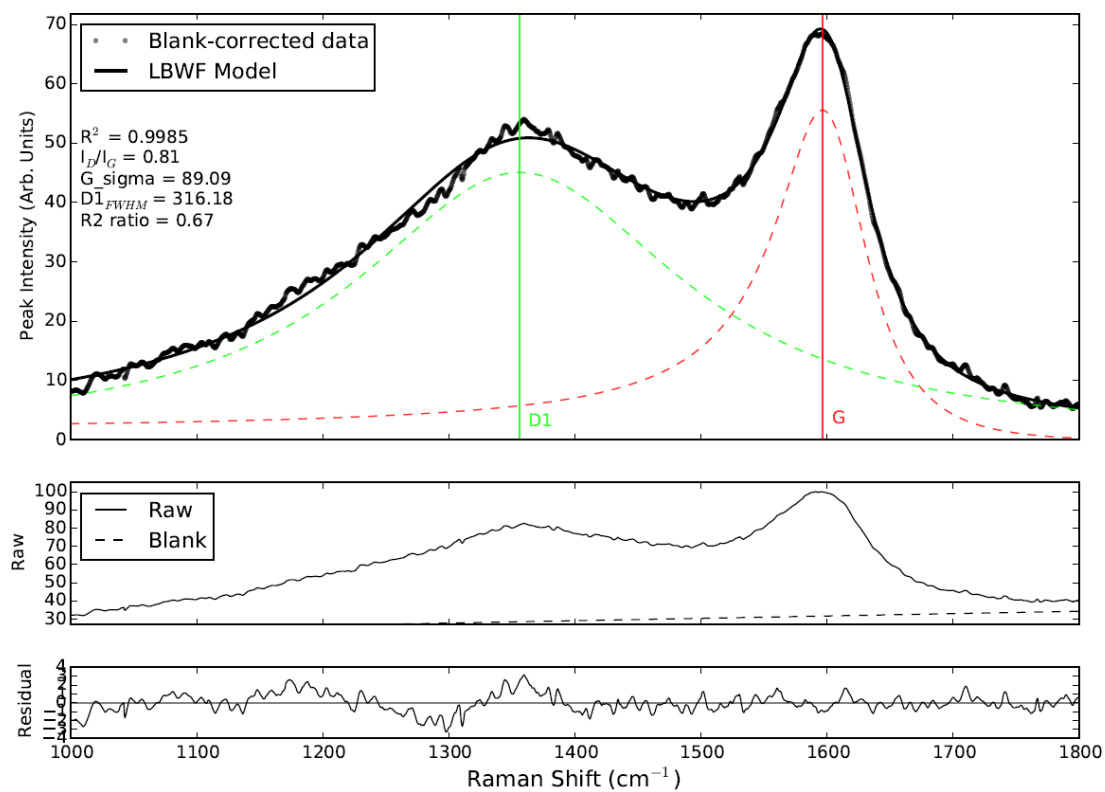


Figure S3. Comparison of the Raman band parameters of the unheated and experimentally-heated Tagish Lake samples obtained by LBWF and 2-Lorentzian (2L) peak-fitting models.

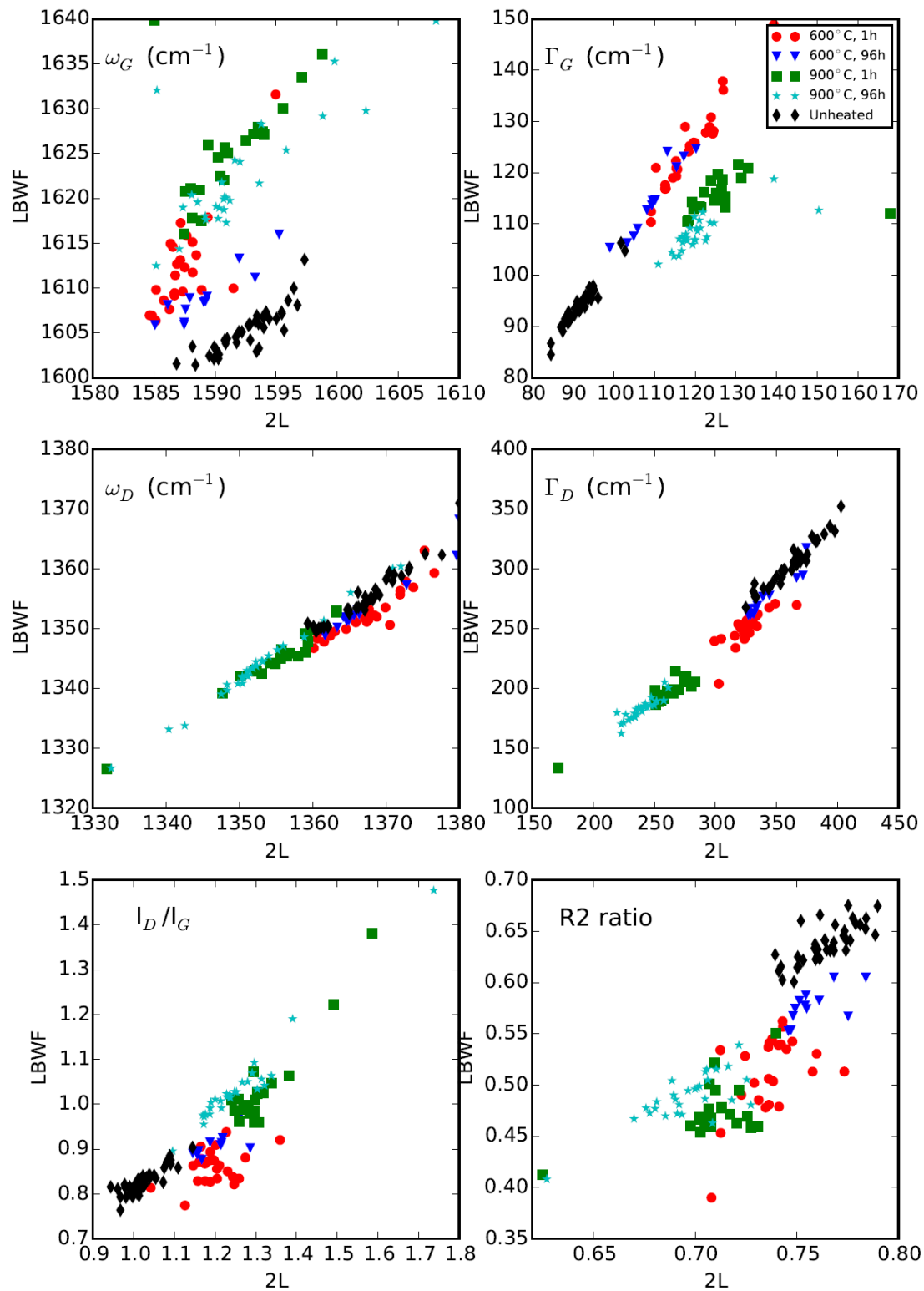


Figure S4. C-XANES spectrum and the spectral fitting procedure from the Tagish Lake meteorite sample (600°C 96h heating experiment) obtained from the FIB section prepared and analyzed on 2016 Feb. The top subplot shows the various Gaussian functions used to model the absorption of known functional groups and their set and actual fitted peak center locations. The middle subplot shows the arctangent function used to model the absorption edge. The bottom subplot shows the spectral fitting residue.

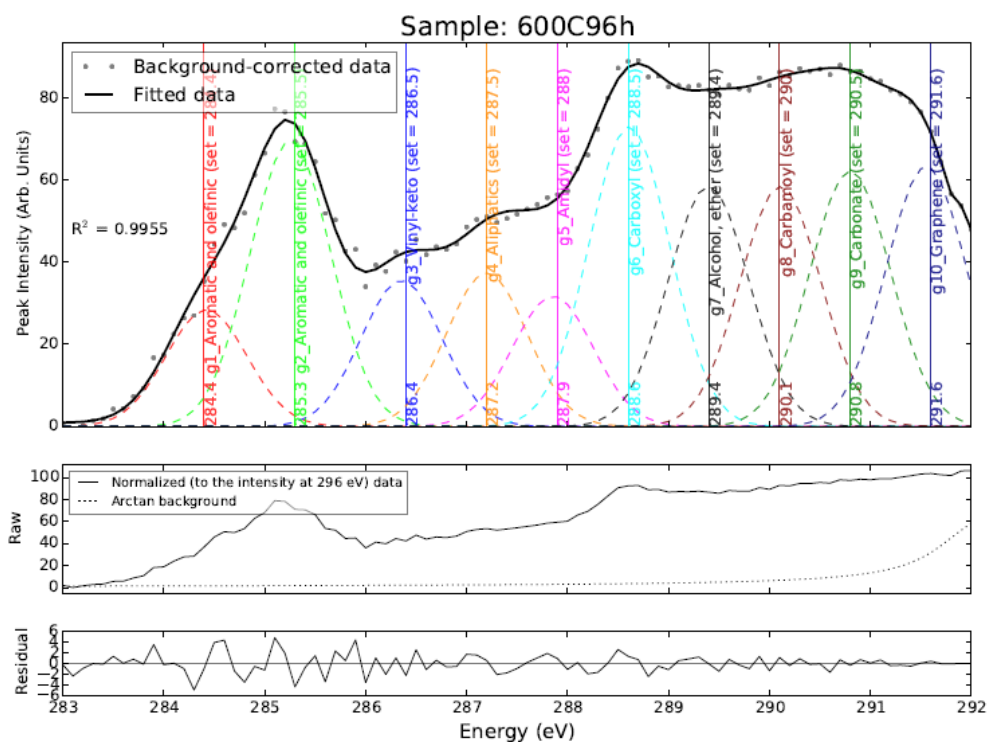


Figure S5. Comparison of the signal intensity between the raw Raman spectra of the unheated and heated Tagish Lake meteorite samples.

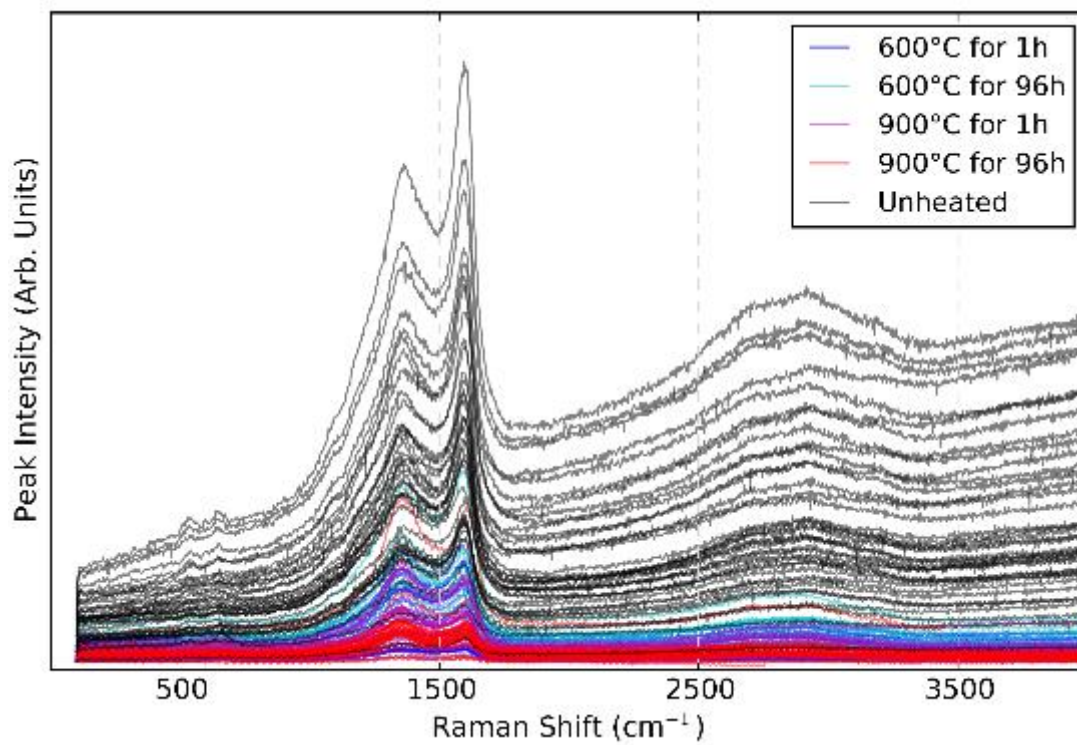


Table S1. Comparison between the Raman peak parameters of the Tagish Lake meteorite between different studies.^a

	ω_G	ω_D	Γ_G	Γ_D	I_D/I_G	Peak fitting model
Quirico et al. 2014	1590.6 ± 3.0	1371.1 ± 4.1	102.9 ± 5.6	247.1 ± 10.3	0.80 ± 0.05	LBWF
Busemann et al. 2007	1580.6 ± 0.2	1350.5 ± 0.2	94.7 ± 0.1	311.4 ± 0.2	1.02 ± 0.05	2-Lorentzian
Matrajt et al. 2004	1593.9 ± 1.5	1378.8 ± 7.3	88.6 ± 7.5	328.1 ± 19.2	0.85 ± 0.06	2-Lorentzian
Nakamura et al. 2002	1591.8 ± 0.9	1381.5 ± 2.6	86.0 ± 3.3	283.9 ± 12.6	2.61	2-Lorentzian
This study	1605.3 ± 2.5	1355.2 ± 4.4	94.2 ± 4.0	304.9 ± 18.7	0.83 ± 0.02^b	LBWF

^aUncertainties are 1σ standard deviation of the mean.

^bThe uncertainty for I_D/I_G represents the propagation of error.

1
2
3 Movie S1. Stack of the two-dimensional (2D) axial images of the Tagish Lake meteorite
4 sample (#11).
5
6
7
8
9
10
11
12
13
14
15
16
17
18
19
20
21
22
23
24
25
26
27
28
29
30
31
32
33
34
35
36
37
38
39
40
41
42
43
44
45
46
47
48
49
50
51
52
53
54
55
56
57
58
59
60

For Peer Review Only

1
2
3
4
5
6
7
8
9
10
11
12
13
14
15
16
17
18
19
20
21
22
23
24
25
26
27
28
29
30
31
32
33
34
35
36
37
38
39
40
41
42
43
44
45
46
47
48
49
50
51
52
53
54
55
56
57
58
59
60

Movie S2. 3D volumetric reconstruction of the Tagish Lake meteorite sample (#11).

For Peer Review Only

Dear Drs. Jull and Sandford,

Thank you very much for handling the editorial process of our manuscript. We have considered all of the comments provided by the reviewer, and revised our manuscript accordingly. Below, please kindly find our point-by-point responses to the suggestions and comments on our manuscript.

Yours sincerely,



Queenie Chan

Our responses to Dr. Cody's comments:

- 1) Note that on Page 23 line 624 it is noted that Cody et al. 2008 flash heated to 600, 1000, and 1400 °C for 2 seconds in helium- this is correct, but they also did long term heating at 600, 800, 1000 and 1200 in argon up to 6 hours.
 - We have modified the sentence into the following:
 - "As noted by Cody et al. (2008b), Murchison IOM samples flash heated for up to two seconds at 600°, 1000°, and 1400°C in helium, and up to six hours at 600°, 800° and 1000°C in argon, all exhibit a systematic increase in the intensity of the 1s-σ* exciton at ~291.6 eV."
- 2) Figure 2: ...review a little about what the mineralogy tells us about the environment during heating, e.g. reducing or oxidizing.
 - We have modified Figure 2 to show the sample before and after the heating experiment of 900°C for 96h (instead of 600°C for 1h) to make it more consistent with the text.
 - We have added the following sentences to the text:
 - "Therefore, while phyllosilicates (e.g. saponite and serpentine), magnetite and Fe-Ni sulfides are common mineral phases observed in the matrix of the carbonate-poor lithology of the Tagish Lake meteorite (Zolensky et al. 2002 MAPS), the Tagish Lake samples heated to 900°C show mineral assemblages of predominantly anhydrous silicates, metal and troilite, implying a reducing heating environment."
 - We have changed the figure legend accordingly:
 - Optical photos of the Tagish Lake meteorite sample before and after the heating experiment at 900°C for 96h. The sample shows significant weight loss (~20%) upon heating which indicates the dehydration of phyllosilicates. Common mineral phases observed in the matrix of the unheated carbonate-poor lithology of the Tagish Lake

meteorite such as phyllosilicates, magnetite and Fe-Ni sulfides were converted into anhydrous silicates, Fe-Ni metal and troilite via dehydration and reduction.

- 3) Figures 3 & 4: "I don't think that anyone really knows exactly what controls D and G band widths, other than higher degrees of crystallinity should favor narrower Raman bands."

"The challenge with Raman has always been that there is no clear functional group level correlation with D and G band features."

"Raman trends are simply trends and are not rigorously tied to specific molecular structural characteristics"

- We have added the following sentences to the text:
 - "The challenge with Raman analysis is that there is no clear functional group level correlation with Raman parameters, unlike XANES analysis which can directly attribute the absorption features to a certain chemical moieties. Therefore, the present data underscore the fact that the trend observed for different Raman parameters of chondritic IOM is not rigorously tied to one specific molecular structural characteristic.
 - Despite the complicated influences of varying molecular structures to the Raman parameters, we can appreciate that a certain structural variation can lead to the development of several trends. One confident link is that higher degrees of crystallinity (ordering) favor the development of sharper bands."
- 4) Clearly there is something different between laboratory heating and natural heating and I suspect it might be confining pressure. I recommend that the authors discuss these unexpected trends in relation to what is observed in naturally thermally evolved IOM.
- We have added a paragraph to discuss immediately after the first mention of the variation between the G parameters of laboratory heated sample and meteoritic IOM (naturally heated sample):
 - "Other than the disparity between the natures of the OM precursors, the difference between the trends observed for the G band parameters of the OM heated under laboratory and natural processes suggests variations in their heating conditions, such as the abovementioned heating kinetics and the confining pressure. IOM metamorphosed naturally at depth on a chondritic parent body up to kms in radius would have an overburden pressure significantly higher than the laboratory experimental condition (Asphaug et al. 2002). High pressure enhances the thermal transformation of organic C by reducing the temperature of graphite formation and accelerating the graphitization process, leading to the formation of graphite through gradual loss of hydrogen and other heteroatoms and annealing of structural defects (Davydov et al. 2004)."

- 5) Note that in Cody et al. 2008 only C-XANES were studied identifying the progressive generation of graphene like features and although C-XANES were compared with

Raman features (for natural samples) no Raman data were collected on the laboratory heated samples. It is quite likely that Raman data on pure IOM heated in the laboratory will show the same confusing G band behavior as seen in the present manuscript.

- We have added the following to the manuscript:
 - “Although Cody et al. (2008b) observed a good correlation between the intensity of the $1s-\sigma^*$ exciton and Raman spectra parameter, the C-XANES data of the experimentally heated IOM samples were compared with previously published Raman data (ΓD and ΓG) of chondritic IOM. Therefore it could be possible that by comparing both the C-XANES and Raman data of the same laboratory heated IOM would give the same trend we observed in this study.”
- 6) Figure 5: I am confused as to why the spectra would change from Feb, May and Dec. The variation is not at all systematic, for example the 900 °C 96 hour looks more like the unheated than do any of the others. The only thing I might suggest is that the differences are more related to variations in beam line characteristics rather than the actual IOM chemistry. (note: we don't actually know how intense the C-XANES spectra are, nor what the base line absorption is- but the S/N suggests that carbon absorption is weak). When C-XANES features are very weak and X-ray beam drift is high (note the X-ray beam can move around), temporal variations in I_0 scans can occur due to variation of carbon back ground on mirrors and monochromator. I would recommend that the authors compare their I_0 scans for those dates to see if there are any differences (the C-XANES spectra are $A = -\log(I/I_0)$ so variation of either “ I ” or “ I_0 ” can change “ A ”).
- We have examined background effect to avoid the dependences of experimental devices and beam quality. All C-spectra were obtained with I_0 at the same time, and subtract the “ I_0 ” from “ I ” after every experiment.
 - We have also cross-checked the I_0 data and confirm that the I_0 data are not the culprit for such variation. Rather the sample heterogeneity is large, sometime even a single FIB section has heterogeneity depending on the ROI.
 - We have discussed the unsystematic variation may reflect the original heterogeneity in the TL sample, since Feb, May, and Dec. samples were prepared from different area in the same heated/unheated sample chip.
 - We have added the following to the manuscript:
 - “The C-XANES spectra were corrected with background and analyzed by the subtraction of a linear regression using aXis2000 software, and then normalized to the intensity at 292 eV.”
- 7) Three diagnostic XAS features: the development of a sharp peak at 291.6 eV and, the development of a pronounced broader peak at 292.3 eV and, the development of graphene-like EXAFS oscillations spanning out to 390 eV +.
- We have added the following to the manuscript:

- 1
2
3
4
5
6
7
8
9
10
11
12
13
14
15
16
17
18
19
20
21
22
23
24
25
26
27
28
29
30
31
32
33
34
35
36
37
38
39
40
41
42
43
44
45
46
47
48
49
50
51
52
53
54
55
56
57
58
59
60
- “In addition to the sharp peak around 291.6 eV, a pronounced broader peak at ~292.3 eV and graphene-like oscillations spanning out to 390 eV in extended X-Ray absorption fine structure (EXAFS) are also indicative of the development of graphene when studying with X-ray absorption spectroscopy (XAS) (G. Cody, personal communication, 2018).”
- 8) A sample of Tagish Lake from an altered clast (probably more similar to 11h- see Herd et al. 2012 and Alexander et al. 2014).
Why TL would behave so differently than Murchison IOM is not clear to me, but It is possible that the highly altered and aromatic rich Tagish Lake (the lithology studied here- more like TL 11v than 5b – see Herd et al) has lost the capacity to transform as Murchison IOM does towards more graphene like material because a lack of aliphatic carbon to begin with. If this is so, then it suggests that different thermal pathways lead IOM to different outcomes.
- We have previously discussed that the TL sample we analyzed is more like the aqueously altered lithology, based on the amino acid content: *“The total amino acid abundance (free + bound) of the identified amino acids in the unheated Tagish Lake sample was about 89 parts-per-billion (ppb), which is consistent with the low amino acid abundance observed for the aqueously-altered lithology of the Tagish Lake sample (sample 11i, 40–100 ppb) and other TMCCs (e.g. Y-980115 ~300 ppb) in the literature”*.
 - We have also discussed the possible explanation for the disparities between the Murchison and Tagish Lake IOM in response to heating. We agree with the reviewer that the low capacity to transform due to the initially high aromatic content of the TL IOM is also a possible reason. In order to emphasize this, we have added the following sentences to the manuscript:
 - “(Tagish Lake specimens showing an increasing degree of aqueous alteration: 5b [the least aqueously altered] < 11h < 11i < 11v [the most aqueously altered])”
 - “The highly aromatic rich nature of the OM suggests that this Tagish Lake sample is more comparable to the aqueously altered specimens such as 11v and 11i rather than 5b analyzed in previous studies (e.g., Herd et al. 2011)”
 - “We discuss here two possible explanations for the Tagish Lake IOM to behave so differently than Murchison IOM. First, the capacity for the highly altered and aromatic-rich IOM in the Tagish Lake sample (comparable to Tagish Lake specimens 11v and 11i) to further transform into graphene like material is limited as there is a lack of aliphatic C to begin with (Figure 5 and Figure 6). Second,”
- 9) Figure 6: It is true that C-XANES can be very subtle. For example if during heating one simultaneously loses aliphatic carbon (reducing intensity at ~ 287.3 eV) while increasing the size of polycyclic aromatic domains (increasing the number of π^* states, then aromatic 1s- n^* intensity will increase across the C-XANES spectrum. That is at energies spanning from 285 eV up to 289 eV. Thus, the apparent lack of trends in peak area ratio, may be hidden by molecular transformation into

polycyclic aromatic hydrocarbons. Note: benzene has 3 π^* states, naphthalene has 5 π^* states, anthracene has 7 π^* states ...etc.

- We agree with the referee on this and have added the following sentences to the main text of the manuscript:
- “Nevertheless, the apparent lack of trends in the peak area ratio may be hidden by molecular transformation into polycyclic aromatic hydrocarbons (PAHs) that shows several resonances at the range of 285–291 eV, in addition to main π^* transition at ~285 eV. For example, the 285–291 eV regions of the C-XANES spectra of benzene (which has 3 π^* states) and anthracene (which has 7 π^* states) are distinct from each other, as benzene has several minor peaks between 287–291 eV in addition to a prominent broad peak at ~285 eV, whereas anthracene is comparatively featureless between 287–291 eV while the main feature at ~285 eV is shown as two smaller peaks at around 284 and 286 eV respectively (Gordon et al. 2003). Therefore, while the intensity at ~287.5 eV is reduced in response to the loss of aliphatic carbon in response to heating, heating also simultaneously increases the size of polycyclic aromatic domains (increasing the number of π^* states) that show different resonances across the 285–291 eV region of the C-XANES spectrum, which could then lead to a non-systematic variation in the peak area ratio.”

10) Figure 7 and Table 1:

These data must be considered with considerable suspicion as it is not at all expected that any amino acids would be detected after heating to 600 °C, let alone 900 °C, for any period of time, let alone 96 hours.

One possibility, is that amino acids actually form from CO, N₂, H₂, ...etc. during cooling from 900 °C to ambient, however, these amino acids (aspartate and glutamic acid) have significant enantiomeric excesses so somehow the formation of such EEs would involve a symmetry breaking that is not at all understood nor predictable.

I can only stress that these results are completely unexpected and if prove to be true, constitute an outstanding result. I would recommend that the authors introduce these data with caution, at least noting that these results are not expected.

- We have added the following discussion to the manuscript:
- “Amino acids can be decomposed at temperatures as low as 100°C (Pietrucci et al. 2018), while proteic-amino acids are typically more thermodynamically unstable than non-proteic amino acids (e.g. β -alanine, γ -aminobutyric acid [γ -ABA]) (Kitadai 2016). Therefore, heating up to 600–900°C is expected to destroy amino acids through processes such as decarboxylation, deamination and chain homolysis which can result in the formation of a variety of simple volatile organic compounds such as amines, carboxylic acids and hydrocarbons (e.g., Bada et al. 1995; Pietrucci et al. 2018; Ratcliff et al. 1974).”
- “These results are completely unexpected as any amino acid present in the samples are susceptible to thermal decomposition at high temperatures. One possibility of

1
2
3 the increase in the amino acid abundance subsequent to heating, is that amino
4 acids are formed from simple precursor molecules such as CO, N₂ and H₂ which
5 serve as feedstock for mineral-catalyzed Fischer Tropsch-type (FTT) reactions (e.g.,
6 Anders et al. 1973; Pizzarello 2012; Yoshino et al. 1971). The FTT reactions lead to
7 the formation of primarily straight-chain amino acids (e.g. glycine, β-alanine, γ-ABA,
8 ε-amino-n-caproic acid [EACA]) of which the amino group is on the carbon farthest
9 from the carboxylic acid. However, when heated to 900°C, the minerals commonly
10 associated with FTT reactions such as montmorillonite clay and magnetite are at
11 expense to form anhydrous silicates, metal and troilite in the Tagish Lake samples
12 (Figure 2). Although metals can also act as FTT reactions catalysts (Dry 2002),
13 hydrogenation of CO to hydrocarbons is a very slow process in the absence of a
14 suitable catalyst (Hayatsu and Anders 1981; Lancet and Anders 1970). The mineral
15 phases of which the formation thresholds are above ~350–400K, such as olivine, Fe
16 and FeS, are not effective catalysts for the FTT reactions, whereas the phases
17 formed at lower temperatures (e.g. montmorillonite clay and magnetite) are. This
18 elucidates a higher abundance of organic compounds in meteorites containing
19 these mineral phases. Therefore, the formation of amino acids via the FTT reactions
20 in the absence of these effective catalysts should be hindered rather than
21 enhanced. When focusing on the yield of the four-carbon amino acids ABA, the
22 abundances of the straight-chain γ-ABA are not always higher than that of the
23 branched isomers in the heated samples (Figure 7), which again testify against the
24 production of amino acids via the FTT reactions.”
25
26
27
28
29
30
31
32
33
34
35
36
37
38
39
40
41
42
43
44
45
46
47
48
49
50
51
52
53
54
55
56
57
58
59
60